Exploring the origin of multi-periodic pulsations during a white-light flare

Dong Li[1,2*], Ding Yuan[3], Jingye Yan[2], Xinhua Zhao[2], Zhao Wu[4], Jincheng Wang[5,6], Zhenyong Hou[7], Chuan Li[8], Haisheng Zhao[9], Libo Fu[3], Lin Wu[2], Li Deng[2]

[1]Purple Mountain Observatory, Chinese Academy of Sciences, Nanjing 210023, China
[2]State Key Laboratory of Space Weather, National Space Science Center, Chinese Academy of Sciences, Beijing 100190, China
[3]Institute of Space Science and Applied Technology, Harbin Institute of Technology, Shenzhen 518055, China
[4]Laboratory for Electromagnetic Detection, Institute of Space Sciences, Shandong University, Weihai, Shandong 264209, China
[5]Yunnan Key Laboratory of the Solar physics and Space Science, Kunming 650216, China
[6]Yunnan Observatories, Chinese Academy of Sciences, Kunming 650216, China
[7]School of Earth and Space Sciences, Peking University, Beijing 100871, China
[8]School of Astronomy and Space Science, Nanjing University, Nanjing 210023, China
[9]Key Laboratory of Particle Astrophysics, Institute of High Energy Physics, Chinese Academy of Sciences, Beijing 100049, China

Key Points:

- Multiple periods are identified in a wide range of radio frequencies, and the used radio telescopes are supported by Chinese Meridian Project.
- A periodicity at about 3 minutes is simultaneously identified in wavelengths of radio, hard X-ray (HXR), Ultraviolet (UV), and Extreme UV (EUV).
- A periodicity at about 8 minutes is simultaneously identified in wavelengths of radio, HXR, EUV/UV, Lyα and white light.

*lidong@pmo.ac.cn

Corresponding author: Dong Li, lidong@pmo.ac.cn

Abstract

We explored the quasi-periodic pulsations (QPPs) at multiple periods during an X4.0 flare on 2024 May 10 (SOL2024-05-10T06:27), which occurred in the complex active region of NOAA 13664. The flare radiation reveals five prominent periods in multiple wavelengths. A 8-min QPP is simultaneously detected in wavelengths of HXR, radio, UV/EUV, Lyα, and white light, which may be associated with nonthermal electrons periodically accelerated by intermittent magnetic reconnection that is modulated by the slow wave. A quasi-period at 14 minutes is observed in the SXR and high-temperature EUV wavebands, and it may be caused by repeatedly heated plasmas in hot flare loops. A quasi-period at about 18 minutes is only observed by STIX, with reconstructed SXR images suggesting that the 18-min period pulsations should be considered as different flares. Meanwhile, a 3-min QPP is simultaneously detected in wavelengths of HXR, radio, and UV/EUV, which is directly modulated by the slow magnetoacoustic wave leaking from sunspot umbrae. At last, a 2-min QPP is simultaneously detected in HXR and radio emissions during the pre-flare phase, which is possibly generated by a quasi-periodic regime of magnetic reconnection that is triggered by the kink wave.

Plain Language Summary

Combined various solar telescopes, especially the radio telescopes supported by Chinese Meridian Project, we analyzed the evolution of multi-wavelength flaring emission during 06:00−07:30 UT on 10 May 2024. Multiple periodicities are identified in the multi-wavelength light curves. A 2-min period is identified in what is described as a precursor event in hard X-ray (HXR) and radio wavelengths. A periodicity at 3 minutes is identified in HXR, radio, Ultraviolet (UV), and Extreme UV (EUV) wavelength observations. A periodicity at 8 minutes is identified in the HXR, radio, EUV, UV, Lyman alpha and white light wavelength observations. Further, a 14-min period is identified in the soft X-ray and high-temperature EUV light curves. Finally, a 18-min period is identified in the low energy soft X-rays. We also tried to explore the origin of these periods based on multi-wavelength observations.

1 Introduction

A flare eruption refers to the impulsive and dramatic electromagnetic radiation over a broad range of wavebands on the Sun and stars, which could be observed in various heights of the solar/stellar atmosphere (see Benz, 2017; Kowalski, 2024, and reference therein). The flare energy is presumably transferred from the free magnetic energy that has been stored in non-potential magnetic configuration in the outer atmosphere (i.e., Shibata & Magara, 2011; X. Yan et al., 2022; Lu et al., 2024). Generally, the flare energy releases explosively and suddenly in a short time via the well-known magnetic reconnection. A portion of the released energy heats coronal plasmas to a higher temperature of several million Kelvin (MK) at the timescale of seconds or minutes, and some other energies rapidly accelerate nonthermal particles to a higher energy in the range from keV to GeV. The majority of accelerated particles could propagate along the newly-formed flare loop and permeate into the lower atmosphere, while a portion of accelerated particles may escape the solar surface and spread into the interplanetary space along open magnetic field lines. Such energy-released process can be well explained by the standard two-dimensional (2D) reconnection model (Priest & Forbes, 2002; Lin et al., 2003). In the spatially-resolved observation of a solar flare, the loop-like features at high temperatures can be clearly seen in wavelengths of Extreme Ultraviolet (EUV) and soft X-rays (SXR). These hot loops are commonly along the closed magnetic field lines and root in the opposite magnetic fields. Two footpoints that are connected by the hot loop are often found in wavebands of hard X-rays (HXR) and microwave, and a loop-top source may appear in HXR and microwave emission (i.e., Masuda et al., 1994; Y. Chen et al., 2017;

Fleishman et al., 2020; D. Li, Warmuth, et al., 2021). Meanwhile, double ribbon-like structures can be observed in the wavelength of ultraviolet (UV), and the flare ribbons often appear as bright kernels in the Hα or white-light emission (Temmer et al., 2007; T. Li et al., 2017; Q. Zhang, 2024). The so-called 'double-ribbons flare' is the most common flare on the Sun, and it matches the standard 2D reconnection model. The solar flare that is observed in the optical continuum channel is usually regarded as the white-light flare (WLF), which is rare event compared to the SXR flare on the Sun, largely due to the strong visible background in the photosphere (Song et al., 2020; Joshi et al., 2021; Fremstad et al., 2023). Therefore, the WLF is often detected in the powerful flare on the Sun (Zhao et al., 2021), or it can be observed in the superflare in solar-type stars (Shibayama et al., 2013; Y. Yan et al., 2021).

The feature of quasi-periodic pulsations (QPPs) is a common phenomenon that is usually associated with the flare radiation in multiple wavelengths. In a broad sense, the QPPs, which are time-dependent oscillations, are often defined as a sequence of repetitive and successive pulsations or pulses in light curves of solar/stellar flares (cf. Zimovets et al., 2021). A typical QPP event should have at least three or four successive pulsations in the time series. It is not necessary to discuss the periodic behavior when there are just one or two pulses, which might be just a coincidence occurred by chance (McLaughlin et al., 2018; D. Li, Li, et al., 2024). The time interval for each pulsation of a flare QPP is expected to be roughly equal, which is termed as the period. However, the majority durations of detected pulsations are always non-stationary, regarded as the quasi-period of non-stationarity QPPs (Nakariakov et al., 2019; Mehta et al., 2023). Their quasi-periods have been reported in a broad range of timescales, i.e., dozens of milliseconds, tens of seconds, and even a few tens minutes (i.e., Tan et al., 2010; Nakariakov et al., 2018; Kashapova et al., 2020; D. Li, Ge, et al., 2021; D. Li et al., 2023; Karlický & Rybák, 2023; Collier et al., 2024; J. Huang et al., 2024; A. R. Inglis & Hayes, 2024; D. Li, 2025). Similar to the flare radiation, the flare QPPs on the Sun can be found in a wide range of wavelengths, such as radio/microwave, white light, Hα, Lyα, UV/EUV, SXR/HXR, and γ-rays (i.e., Milligan et al., 2017; Chelpanov & Kobanov, 2021; D. Li, 2022; D. Li & Chen, 2022; Shen et al., 2022; Zimovets et al., 2023; Shi et al., 2024; Millar et al., 2024; Zhou et al., 2024). On the other hand, the flare QPPs in solar-type stars are often reported in wavebands of white light and X-rays (Kolotkov et al., 2021; Howard & MacGregor, 2022). The quasi-periods measured in solar and stellar flares often depend on the time resolution of the detected telescopes (McLaughlin et al., 2018).

It is still an open issue for the generation mechanism of flare QPPs (Zimovets et al., 2021; A. Inglis et al., 2023). The QPPs behavior can be directly induced by the magnetohydrodynamic (MHD) wave in plasma/magnetic loops, and the eigenmodes may be slow-mode, fast kink- or sausage-mode (Nakariakov & Kolotkov, 2020). The QPPs feature can also be driven by a periodic regime of intermittent magnetic reconnection, and the periodic reconnection might be either triggered or spontaneous (i.e., Karampelas et al., 2023; Comisso, 2024; Kumar et al., 2024; Sharma et al., 2024; Y. Zhang et al., 2024). That is, the periodicity of magnetic reconnection could be caused owing to an external MHD wave, or it might be regarded as a self-oscillation system. In such case, the non-thermal electrons and ions are periodically accelerated by the intermittent magnetic reconnection during the solar flare. So, it is easier to trigger the QPPs feature that is observed in HXR and microwave channels during the impulsive phase of a solar flare (Yuan et al., 2019; Luo et al., 2022; D. Li, Hong, et al., 2024). In a recent review paper (Zimovets et al., 2021), fifteen mechanisms/models are summarized, which are almost according to the MHD waves or the intermittent reconnection model. However, it is still impossible to determine an unambiguous conclusion that which generation mechanism should be responsible for all flare QPPs, largely due to the qualitative nature of generation models and the insufficient information of observational data. That is, it is not yet possible to use one single model to interpret all observed QPPs, and the detected QPPs in different categories could be caused by different mechanisms (McLaughlin et al., 2018; A. In-

glis et al., 2023). Because the available observations can not be fully distinguish from various models.

The observed QPPs show a broad range of quasi-periods, and one QPP event is often dominated by a certain period. The QPPs with double or multiple periods are also reported in a same event (Chowdhury et al., 2015; Karlický & Rybák, 2020). The QPPs at double periods are thought to be dependent on the MHD modes, and they are expected to have a period ratio of about two in the weakly dispersive modes (Nakariakov et al., 2005). However, the observed period ratio often deviates obviously from two, which could be attributed to the highly dispersive modes or some additional physical effects, such as the expansion of plasma loops (Verth & Erdélyi, 2008), or the stratification of longitudinal density (Andries et al., 2005). The flare QPPs with multi-periods could be observed in the same phase or different phases (Hayes et al., 2016; Tian et al., 2016), and multiple periods in a same flare could be detected either in one certain wavelength or in various wavebands (D. Li & Zhang, 2017; X. Chen et al., 2019). Besides these discrete multi-periods, the continuous multi-periods are also discovered in flare QPPs, which often reveal a growing periodicity with time, and the growing periods could be associated with the length of flare loops (Reznikova & Shibasaki, 2011; Pugh et al., 2019; D. Li, Ge, et al., 2021). The idea is that the reconnection site moves toward higher altitudes, therefore, the flare loops become longer and their footpoints, i.e., the flare ribbons, moving away from each other.

One critical issue is to understand the generation mechanism of flare QPPs at multiple periods. In this article, we explored the QPPs feature with multiple periods during a powerful solar flare, we also tried to explore their generation mechanisms. The article is organized as follows: Section 2 describes the observations, Section 3 introduces the data reduction and our main results, Section 4 provides some discussions, and a brief summary is shown in Section 5.

2 Observations

On 2024 May 10, a powerful solar flare occurred in the active region of NOAA 13664, which was a super active region and produced a number of major flares (Y. Li et al., 2024). The target flare occurred near a group of sunspots, and it was simultaneously observed by various instruments: the Atmospheric Imaging Assembly (AIA; Lemen et al., 2012), the Helioseismic and Magnetic Imager (HMI; Schou et al., 2012), and the Extreme ultraviolet Variability Experiment (EVE; Woods et al., 2012) for the the Solar Dynamics Observatory (SDO), the Solar Ultraviolet Imager (SUVI) and the X-Ray Sensor (XRS) carried by the Geostationary Operational Environmental Satellite (GOES), the Spectrometer/Telescope for Imaging X-rays (STIX; Krucker et al., 2020) on board the Solar Orbiter, the Gravitational Wave High-Energy Electromagnetic Counterpart All-sky Monitor (GECAM; Xiao et al., 2022), the Hard X-ray Imager (HXI; Y. Su et al., 2019) and the Lyα Solar Telescope (LST; L. Feng et al., 2019) for the Advanced Space-based Solar Observatory (ASO-S; Gan et al., 2019; Y. Huang et al., 2019), the New Vacuum Solar Telescope (NVST; Liu et al., 2014; X. Yan et al., 2020), the Solar Upper Transition Region Imager (SUTRI; Bai et al., 2023), the Chinese Hα Solar Explorer (CHASE; C. Li et al., 2019), the Chashan Broadband Solar radio spectrometer (CBS; Shang et al., 2022; F. Yan et al., 2023), the STEREO/WAVES (SWAVES; Kaiser et al., 2008), the Large-Yield RAdiometer (LYRA) on board the PRoject for OnBoard Autonomy 2 (Dominique et al., 2013), the Nobeyama Radio Polarimeters (NoRP), and the DAocheng Solar Radio Telescope (DART; J. Yan et al., 2023; R. Li et al., 2024).

SDO/AIA captures EUV/UV snapshots nearly simultaneously with a temporal cadence of 12/24 s in EUV/UV wavebands, SDO/HMI provides the line-of-sight (LOS) magnetogram and visible continuum maps near the Fe 6173 Å line at a temporal cadence of 45 s, and they have a same spatial scale of $0.6''$ pixel^{-1} after processing by a standard

procedure. SDO/EVE records the EUV spectrum for the entire Sun in the wavelength range of about 1−1216 Å. Some emission lines at EUV and Lyα can be extracted from the EUV spectrum, and their temporal cadence is averaged down to 60 s. GOES/SUVI probes the corona that includes million-degree temperature, which has a temporal cadence of ∼120 s, and a spatial scale of 2.5″ pixel^{-1}. GOES/XRS records the SXR fluxes integrated over the whole Sun in 1−8 Å and 0.5−4 Å at a temporal cadence of 1 s. Based on their ratio, the iso-thermal temperature could be estimated (White et al., 2005). LYRA records the solar irradiance at four wavebands at a temporal cadence of 0.05 s. STIX provides the flare imaging spectroscopy of solar flares in the X-ray range of 4−150 keV at a temporal cadence of about 0.5 s. GECAM can measure solar irradiance in X- and γ-rays. In this case, the solar X-ray flux at about 18−48 keV was used, which has a temporal cadence of 1 s.

ASO-S/LST equipped with two telescopes: the Solar Disk Imager (SDI) and the White-light Solar Telescope (WST). SDI takes the Lyα maps with a normal cadence of 60 s, and it changes to ∼6 s in flare mode. WST provides the white-light map at 3600 Å in a normal cadence of 120 s, and it can reach to ∼1 s in the flare mode. HXI provides the imaging spectroscopy of solar flares in HXR channels of about 10-300 keV. The temporal cadence is normally 4 s, and it can be as high as 0.125 s in the flare mode. NVST, which situates at Fuxian Lake, can provide the localized images in channels of Hα and TiO-band. In this case, the TiO images with a FOV of 133″×112″ were provided, and it has a spatial scale of 0.052″ pixel^{-1} and a temporal cadence of ∼30 s. CHASE operates the spectroscopic observation of the entire Sun in wavelength ranges of Hα and Fe I at a temporal cadence of about 71 s and a spatial scale of 1.04″ pixel^{-1}. SUTRI takes the EUV map at a temperature of ∼0.5 MK (Tian, 2017), which has a temporal cadence of ∼31 s and a spatial scale of 1.23″ pixel^{-1}. Noting that the CHASE and SUTRI maps are discontinuous due to the orbit period, and they missed the impulsive phase of the major flare.

The DART Radiaheliograph routinely produces solar radio snapshots from 149 MHz to 447 MHz. The spatial scale is about 52″ pixel^{-1} in the frequency of 447 MHz, and it decreases to about 157″ pixel^{-1} at 149 MHz, while it has a uniform temporal cadence of 10 s. CBS is a newly built solar radio spectrograph at Chashan Solar radio Observatory (CSO). It provides solar radio dynamic spectra in a broad frequency range of millimeter (∼35−40 GHz, mm), centimeter (∼6−15 GHz, cm), decimeter (∼0.5−6 GHz, dm), meter-decameter (∼80−610 MHz, m) regimes. Their temporal cadences are ∼0.53 s (CBSmm), ∼0.067 s (CBScm), ∼2.15 s (CBSdm), and ∼0.1 s (CBSm), respectively. DART and CSO are both solar radio telescopes supported by Chinese initiative Meridian Project phase 2. SWAVES takes the solar radio spectrum in the low frequency range of ∼0.0026−16.025 MHz at a temporal cadence of 60 s. NoRP measures solar radio fluxes in six microwave frequencies at a temporal cadence of 1 s.

3 Data reduction and results

The target flare was measured by various instruments, which provided us an opportunity to investigate the flare QPPs at multiple periods in multiple wavelengths, i.e., HXR/SXR, EUV/UV, white light, Lyα, and radio.

3.1 Overview of the powerful flare

Figure 1 presents an overview of the target flare on 2024 May 10. Panel (a) shows the full-disk light curves in SXR and X-ray ultraviolet (XUV) wavebands from 06:00 to 07:30 UT. The GOES 1−8 Å flux suggests an X4.0-class flare, it started at about 06:27 UT, reached its maximum at about 06:54 UT, and stopped at about 07:13 UT, as marked by the vertical dashed lines. The GOES fluxes at 1−8 Å and 0.5−4 Å reveals three successive pulsations from about 06:18 to 07:00 UT, indicating a QPP signal in the SXR

channel, and it is much more visible in the temperature profile, suggesting that it highly depends on periodic variations of the plasma temperature. The STIX flux at 4-10 keV also shows three successive pulsations during ∼06:01−06:59 UT. Obviously, the QPP period is longer than that observed by GOES. Conversely, XUV flux at 1−800 Å recorded by LYRA appears a rather weak signal of QPP.

In Figure 1(b), we show the light curves in channels of HXR and microwave measured by HXI and NoRP, which also appear a number of successive pulsations. However, they are different from those successive pulsations in the SXR channel. Moreover, at least three successive pulsations with a small amplitude are seen in the HXR channel, as indicated by the green arrow. They appear before the onset of the X4.0 flare, which might be regarded as a precursor. Panels (c)−(e) show EUV maps observed by GOES/SUVI during the flare impulsive phase, and they have a large FOV. The over-plotted blue contours represent the HXR radiation, which are reconstructed by the HXI_CLEAN algorithm from the HXI data between 06:42−06:44 UT. The flare sources seen in wavebands of HXR and EUV match with each other. We also plot the radio sources in the meter-wave regime measured by DART, as shown by the color contours in panels (d) and (e). The radio sources are far away from the flare area. The distance between the radio source and the flare site becomes farther with the observed frequency decreasing, but the radio source region becomes larger and larger. This feature could be attributed to the angular resolution of DART, that is, the angular resolution of DART becomes lower and lower with the decreasing of radio frequencies. Or it may be due to the high loop top (Gary et al., 2018).

Figure 2 shows the dynamic radio spectra measured by CSO Radiaheliograph and SWAVES in a wide range of frequencies. The over-plotted curve in each panel represents the radio flux at the designated frequency, as marked by the short line on the left hand. A sequence of radio bursts can be seen in the dynamic spectra, and they drift rapidly from higher to lower frequencies, which might be regarded as a group of centimeter-decimeter bursts, as shown in panels (a)−(e). On the other hand, some radio bursts only appear in the meter-decameter regime (panel d), and they are almost no frequency drift, which might be considered as the type IV burst. A type III group is seen in the low frequency range measured by SWAVES, as shown in panel (e). Anyway, all these radio emissions seem to show quasi-periodicity. The overlaid fluxes show a number of successive pulsations, especially for the radio fluxes in frequencies of 7.95 GHz, 3.96 GHz, 300 MHz, and 1.575 MHz. Conversely, the radio flux at 37.75 GHz show a weak signal of QPP, which may be attributed to its higher frequency, and thus it requires a large amount of energies.

3.2 Multi-periodic pulsations

In order to determine the quasi-period of flare QPPs, we perform the fast Fourier Transform (FFT) for the raw light curves with a Lomb-Scargle periodogram method (Scargle, 1982), and the confidence level is defined by Horne and Baliunas (1986). Figure 3 presents the FFT power spectra in multiple wavebands, the cyan curve represents the best fit result for the observational data, and the magenta curve is the confidence level at 99%. We can find that several peaks exceed the 99% confidence level, especially in wavebands of radio and HXR (a-d), as indicated by the color arrows. However, some peaks only appear in one or two wavebands (hot pink arrows), so they are not considered in this study. At last, three dominant periods (P1-P3) are simultaneously identified in NoRP 3.75 GHz, HXI 20-50 keV, CBS 300 MHz and CBS 7.95 GHz, as indicated by the green arrows. For simple, the three dominant periods are regarded as 2-, 3-, and 8-minutes, respectively.

In Figure 3 (e) and (f), we also show the FFT power spectra in the SXR channel. From which, a dominant period of about 14 minutes (P4) appears in the time series of GOES temperature, and a dominant period of about 18 minutes (P5) exceeds the con-

fidence level in the energy range of STIX 4-10 keV. The FFT results are consistent with the three pulsations in raw light curves measured by GOES and STIX in Figure 1, confirming the existence of 14-min and 18-min QPPs.

3.3 Local observations

The radio dynamic spectra and HXR/SXR fluxes are all integrated over the whole Sun. To search for the source region that generated the flare QPPs, we draw the multi-wavelength images in Figures 4 and 5. Figure 4 shows the EUV/UV images and the line-of-sight (LOS) magnetogram with a same FOV of about $270'' \times 270''$ during the X4.0 flare. Two groups of hot loops (pink arrows) can be clearly seen in wavebands of AIA 94 Å and 131 Å at about 06:36 UT, and they become a bright loop and several weak loops at about 06:51 UT, as marked by the red arrow. The hot loop can be seen in AIA 193 Å, but it is hard to be observed in AIA 211 Å, suggesting that the flare loop is filled with high-temperature plasma, i.e., >6 MK. Some bright kernels appear in AIA 304, 1600 and 1700 Å, and SUTRI 465 Å at about 06:36 UT, and they become double ribbons (RB1 and RB2) at about 06:51 UT. The HXR emissions observed by HXI 20-50 keV are overlaid on AIA 131 and 1600 Å maps, and they are mainly situated in double ribbons, named as footpoints, as shown by the blue contours. The footpoints/ribbons connected by hot loops have changed from about 06:36 UT to 06:51 UT, implying that the magnetic reconnection occurs during the X4.0 flare. A weak signature of dark structure is simultaneously found in wavebands of AIA 193, 211, and 304 Å at about 06:36 UT, as indicated by the green arrow. The dark structure can be clearly seen in wavebands of AIA 171 Å before the X4.0 flare, i.e., at about 06:00 UT. Moreover, a sunspot group can be found in AIA 1600 nd 1700 Å, which locates in a complex magnetic field structures (panel i). All these observations suggest that the dark structure could be regarded as a micro-filament, and the magnetic reconnection during the X4.0 flare could be triggered by the filament eruption. The gold box outlines the flare area used to integrate over the local flux in EUV/UV wavelengths.

Figure 5 shows some more sub-maps in multiple wavelengths during the X4.0 flare. In panels (a)-(c), one patch of visible continuum enhancement is simultaneously detected in wavebands of WST 3600 Å, HMI continuum near 6173 Å, and NVST TiO 7058 Å, as outlined by the magenta contour. Thus, the X4.0 flare can be regarded as a WLF, and the gold rectangle outlines the flare area used to integrate the white-light flux. Moreover, the white-light brightening is temporally and spatially consistent with the HXR radiation source, as marked by the blue contours. The cyan contours outline the boundary between the umbra and penumbra. Panels (d1)-(d3) shows the Hα images at its line center and two line wings measured by CHASE at about 06:56 UT. The radiation enhancements seen in two line wings of Hα (d1 and d3) appear to match the white-light brightening, suggesting that the Hα line-wing radiation is mostly from the upper photosphere to the lower chromosphere. Similar to the AIA 304 Å image, the Hα image at its line center (d2) reveals double ribbons. Figures 5 (e)-(g) presents the EUV sub-maps observed by SUTRI 465 Å, AIA 171 and 335 Å at about 07:19 UT. They both show a number of loop-like structures, which could be regarded as the post flare loops.

In Figure 6, we show multi-wavelength light curves, and they are normalized by their maximum intensity. Panel (a) presents the full-disk light curves recorded by SDO/EVE for the isolated lines, including high- (Fe XX, Fe XIX) and low-temperature (Ne VII, He I and H I) lines. Panel (b) shows the local light curves measured by SDO/AIA, which are integrated over the flare area. The local AIA fluxes are also divided into high- (131 and 94 Å) and low-temperature (1600, 304 and 1700 Å). The time series at high-temperature channels show the quasi-period that is consistent with the SXR fluxes recorded by GOES. Conversely, the time series at low-temperature channels appear to reveal multi-period QPPs, which agree with the HXR and radio fluxes. Moreover, the precursor pulse can also be seen in the local AIA fluxes, as marked by the green arrow, confirming the pres-

ence of flare precursor. Figure 6 (c) shows the white-light fluxes measured by WST 3600 Å, HMI continuum, and NVST TiO, which are integrated over the WLF region. Here, we also show the local flux in SDI 1216 Å, and the full-disk light curve in EVE 1210-1220 Å. They match with each other, regarded as the Lyα flux. All these time series in wavebands of white light and Lyα also reveal a prominent signature of quasi-periodicity. Figure 6 (d) presents the local radio fluxes at meter-wave regime, which are measured by DART. They all appear the QPP feature with multiple periods. All these observational results are similar to that obtained from the FFT power spectra in Figure 3.

3.4 Precursor QPP

The local fluxes measured by SDO and ASO-S demonstrated the existence of the flare precursor. Figure 7 presents the light curves (a and b) and images (c-e) in multiple wavelengths during the pre-flare phase, i.e., from 06:10 UT to 06:30 UT. The HXR light curves in the energy range of HXI 20-50 keV and GECAM 18-48 keV show four successive peaks (1-4) during ∼06:17-06:25 UT, within an average duration of about 2 minutes. The average duration is consistent with the 2-min period (P1) detected in radio and HXR channels, which may be regarded as the precursor QPP. The precursor QPP can be seen in radio/microwave fluxes in frequencies of NoRP 9.4 GHz and CBS 7.95 GHz, and it shows a weak QPP signature in the local light curves in wavelengths of AIA 1600 Å and SDI 1216 Å. However, it is hard to see any QPP feature in channels of AIA 131 Å, Ne VII 465 Å (EUV), DART 300 MHz, and CBS 300 MHz (meter-wave). These intensity curves only show one apparent pulse during the precursor, and the pulse seen in the meter-wave regime is shorter/narrower and earlier than that observed in the EUV wavelengths. This observational fact also implies that the flare precursor is highly related to the nonthermal electrons, and the precursor QPP could be driven by a quasi-periodic regime of magnetic reconnection. Panels (c)-(e) show the EUV/UV sub-maps with a same FOV of about $400''\times400''$ during the flare precursor. Similarly to what has seen in the X4.0 flare, some hot loop-like features can be found in the high-temperature channel of AIA 131 Å, and some ribbon-like structures are seen in the low-temperature channel of AIA 1600 Å, SDI 1216 Å (tomato), and SUTRI 465 Å (cyan). Moreover, some bright kernels (blue) are measured by HXI 20-50 keV, and they appear to be connected by hot loops, termed as footpoints. At last, the radio source measured by DART 300 MHz seems to be far way from the precursor region, which may be attributed to the high loop top.

4 Discussions

The X4.0 flare shows QPP behaviors at multiple periods in various wavebands during different flare phases. In order to reveal their trigger mechanisms, we used the wavelet transform and Fourier transform to determine the temporal and spatial distributions of multi-period QPPs.

4.1 Temporal distribution

In order to identify the temporal distribution of the flare QPPs, we performed the wavelet transform with a 'mother' function (Torrence & Compo, 1998) for the detrended time series. This method can well resolve the temporal distribution of periods, that is, the time-resolved period. However, it is often used for the detrended time series, which might introduce a spurious periodicity in signals (Broomhall et al., 2019). In this study, two running windows are used for each raw light curve to obtain the detrended time series, and thus the artifact period of the detrending process could be excluded (i.e., Tian et al., 2012; D. Li, Wang, & Huang, 2024). The time resolution of light curves measured by WST 3600 Å and SDI 1216 Å is nonuniform due to the switch of observational modes. Therefore, the white-light and Lyα fluxes are interpolated into the unform time resolutions of 120 s and 60 s, respectively. Figure 8 shows the Morlet wavelet analysis results

for multi-wavelength light curves. Considering the broad period range of QPPs, different running windows are used for various channels. Panels (a1)-(f1) show the Morlet wavelet power spectra in wavebands of radio, HXR, white light, Lyα, and low-temperature EUV/UV during the X4.0 flare, and they are characterized by a bulk of power spectra inside the 99% significance level. Panels (a2)-(f2) presents the global wavelet power spectra with two running windows of 10 (black) and 15 minutes (magenta), respectively. They all reveal a prominent peak that is centered at about 8 minutes, confirming the presence of the 8-min period (P3). On the other hand, the global wavelet power spectra measured by CBS 3.96 GHz, HXI 20-50 keV, SDI 1216 Å, and AIA 1600 Å display another peak that is centered at about 3 minutes, although the signature of 3-min QPP in wavebands of SDI 1216 Å and AIA 1600 Å is a bit weak. All these results provide prominent observational signatures of the existence of the 3-min period (P2). On the contrary, the 3-min period is not observed in wavebands of WST 3600 Å and EVL 465 Å, largely due to their lower temporal resolution, i.e., 2 minutes.

Panels (g1) and (g2) present the Morlet wavelet power spectrum and its global wavelet power spectrum in the wavelength of high-temperature EUV from the precursor to X4.0 flare. Here, the running windows of 15 (black) and 20 minutes (tomato) are used, as we expected a 14-min period. The power spectrum shows a broad range of period at a center of about 14 minutes, which is similar to the 14-min period (P4) in SXR channels. Panels (h1)-(h2) show the Morlet wavelet power spectrum and its global wavelet power spectrum in the channel of HXR during the precursor. The running windows of 3 (black) and 5 minutes (hot pink) are used, since the 2-min and 3-min periods are expected. Double peaks that are centered at 2 minutes and 3 minutes can be seen in the global wavelet power spectrum, similar to the P1 and P2 periods. The wavelet analysis results suggest that the 2-min period is mainly from the precursor phase, which might be regarded as a precursory indicator of the powerful flare (Tan et al., 2016; D. Li et al., 2020).

4.2 Spatial distribution

In order to determine the trigger source of flare QPPs at various periods in multiple wavelengths, that is, spatial-resolved their sources, the Fourier transform (i.e., A. R. Inglis et al., 2008; R. A. Sych & Nakariakov, 2008; S. Feng et al., 2020) is performed on the radiation intensity of every pixel in several channels, as shown in Figure 9. Panel (a1) shows the visible continuum map measured by SDO/HMI before the X4.0 flare. It reveals a group of sunspots, the umbras and penumbras are clearly distinguished, as indicated by the magenta contours. Panel (a2) presents the spatial distribution of the normalized Fourier power that is averaged over the spectral component at 2-4 minutes for the HMI continuum data during 06:00-08:00 UT, containing the flare and non-flare time. We can find that the spectral component at the period range of 2-4 minutes is generally situated in sunspot umbras, as outlined by the magenta contours. Panel (b) presents the magnetic configuration on the flare active region, and it is derived from the potential field source surface (PFSS) extrapolation (Schrijver & De Rosa, 2003). The flare active region is filled with a number of magnetic field lines, including the open and closed lines, as indicated by the purple and white lines, respectively. Also, the flare area and the sunspot umbra are linked by some magnetic field lines, providing an opportunity for the propagation of slow waves from sunspot umbras to the flare area. This model was first presented by Nakariakov and Zimovets (2011), who proposed that the QPPs of double-ribbon flares could be explained by propagating slow waves. Then, it is demonstrated by studying the relationship between HXR pulses and footpoint sources in double-ribbon flares (A. R. Inglis & Dennis, 2012). And the slow wave has been used to explain the 3-min QPP in HXR, microwave, UV, and Lyα emissions (cf. D. Li, Hong, et al., 2024), similar to the 3-min period in our case.

Figures 9 (c1) and (d1) show the UV/EUV sub-maps in wavelengths of AIA 1600 and 94 Å during the X4.0 flare. Double flare ribbons can be seen in the low-temperature

waveband of AIA 1600 Å, and hot flare loops are observed in the high-temperature waveband of AIA 94 Å, as marked by the cyan and tomato contours. Panels (c2) and (c3) present the spatial distributions of normalized Fourier power for the AIA 1600 Å data, and they are averaged among 2-4 and 7-9 minutes during 06:15-07:15 UT. We can find that the Fourier power spectra are significantly enhanced in the double flare ribbons, including the spectral components at 2-4 and 7-9 minutes. Panels (d2) and (d3) shows the spatial distributions of normalized Fourier power for the AIA 94 Å data, which are averaged among 2-4 and 13-15 minutes during the same time interval. The spectral component at 2-4 minutes appears to enhance at double flare ribbons or footpoints, while that at 13-15 minutes appears at the hot flare loops. The spectral component at 2-4 minutes is similar to the quasi-period at 3 minutes, and it can be simultaneously observed in wavebands of HXR, radio, EUV/UV, and Lyα at double ribbons or footpoints. Moreover, the similar period of 3 minutes is detected in the adjacent sunspot umbras, and the flare ribbons and the sunspot umbras are connected by some magnetic field lines. All those observations support that the 3-min QPP is most likely modulated by the slow magnetoacoustic wave leaking from the sunspot umbra (i.e., Yuan et al., 2011; R. Sych et al., 2009; A. R. Inglis & Dennis, 2012; Kumar et al., 2016; D. Li, Hong, et al., 2024). The idea is that the slow magnetoacoustic wave at about 3 minutes is always existent in the sunspot umbras, it originates from the photospheric umbra, and then propagates along the magnetic field lines, causing the flare QPP at about 3 minutes in the outer solar atmosphere (i.e., Nakariakov & Zimovets, 2011; Yuan et al., 2014; Yuan, 2015; R. Sych et al., 2024), as illustrated in Figure 11 (a). The spectral component at 13-15 minutes is similar to the quasi-period at 14 minutes seen in wavelengths of SXR and high-temperature EUV, which may be associated with the periodic variation of high-temperature plasmas that is heated by the loop-loop interaction (D. Li, Li, et al., 2024), as the 14-min period is mainly located in hot flare loops. We also note that the three main peaks seen in the GOES flux originate from the same active region however they appear to originate from different parts of the active region, which are linked by some interaction between the magnetic fields of loop systems in the active region. This also confirms that the temperature evolution at a period of 14 minutes is attributed to the loop-loop interaction. Moreover, the 14-min period can be only detected in wavebands of SXR and high-temperature EUV, implying that it depends on temperature.

Figure 10 (a) shows the spatial location of the Solar Orbiter with respect to Earth at 06:45 UT on 2024 May 10. STIX was located at about 166.9 degree west in solar longitude from the Sun-Earth line, their distance was about 0.69 AU. Thus, STIX observed the Sun at a different point, comparing the Earth's perspective. Panels (b)-(d) presents the SXR images at three time intervals, corresponding to the three pulsations in the STIX light curve. The SXR images at 4-10 keV are reconstructed from the STIX pixelated science data in the STIX Aspect System (Warmuth et al., 2020). For validating the source location of the reconstructed SXR emissions, three image reconstruction methods that have been implemented in the STIX data analysis software are used, that is, the expectation-maximization algorithm (EM), the back-projection method (BP), and the maximum entropy method (MEM_GE). The source locations of the second and third pulsations match with each other, but they are far away from that of the first pulsations. Moreover, the first pulsation locates inside the solar limb, so it was not observed by GOES and SDO/AIA in the Earth measurement. Thus, the quasi-period at about 18 minutes is only observed in the channel of STIX 4-10 keV, which could be attributed to the intermittent energy-release processes of different solar flares. That is, these three pulsations are different in the space, but they are successive and repetitive in the term of time series. Therefore, we still termed it as the 18-min period, since they are flare emissions with similar time intervals between three successive pulses (Zimovets et al., 2021), although they are in fact different flares.

We wanted to discuss the generation mechanism of the quasi-period at about 8 minutes. These pulsations can be simultaneously seen in wavebands of HXR, radio, EUV/UV,

white light, and Lyα emissions. Moreover, it can be detected in a broad range of radio frequencies, ranging from the centimeter through the decimeter to the meter-decameter regimes. All these observations suggest that the 8-min period could be associated with nonthermal electrons that are periodically accelerated by intermittent magnetic reconnections, i.e., the periodic regimes of repetitive magnetic reconnection. The idea is that the flare radiation in wavelengths of HXR, radio, white light, and Lyα are usually related to accelerated electrons via the well-known magnetic reconnection (Priest & Forbes, 2002; Lin et al., 2003). Therefore, the nonthermal electrons can be periodically accelerated during the X4.0 flare, causing the 8-min QPP simultaneously in wavelengths of HXR, radio, white light, and Lyα emissions, as illustrated in Figure 11 (b). This is also consistent with the white-light QPP reported in an X8.2 flare (Zhao et al., 2021). On the other hand, D. Li, Wang, and Huang (2024) reported a white-light QPP at the period of about 8.5 minutes, but it was only observed in the white-light emission. This is obviously different from the 8-min period observed in multiple wavelengths in our case. Therefore, the 8-min QPP can not be modulated by the slow-mode magnetoacoustic gravity (MAG) wave originating from the sunspot penumbra. If the slow-mode MAG wave at the period of about 8 minutes is originated in the solar lower atmosphere, then it cannot propagate upwardly into the solar upper atmosphere, due to the low-frequency cutoff in the photosphere (R. Sych et al., 2009; J. T. Su et al., 2013; Yuan et al., 2014; Kumar et al., 2016). That is, only the 3-min period wave can propagate upwardly to the solar outer atmosphere, and the quasi-period at about 3 minutes seen in double ribbons can well be explained by the slow magnetoacoustic wave, as it can be simultaneously observed in multi-height solar atmospheres, as shown in Figure 11 (a). Moreover, the 3-min period can be simultaneously seen in multiple AIA wavelengths, e.g., high- and low-temperature channels, suggesting that the slow wave is independent of temperature, which is similar to our previous findings (D. Li, Hong, et al., 2024).

4.3 Coronal seismology and scaling laws

Given the wide range of wavelengths considered, the flare QPPs at multiple periods can be applied for the coronal seismology. That is, the multi-period QPPs are useful for diagnosing the key parameters of the flaring core, since they carry the time characteristics of flare radiation (Pugh et al., 2019; Yuan et al., 2019). The flare QPPs could be a novel tool to diagnose the stellar atmospheres if their generation mechanisms are justified, because the spatial resolution of a remote star is difficult to achieve (Zimovets et al., 2021; Kowalski, 2024). In our case, the 2-min QPP is explained by the periodic magnetic reconnection. The idea is that nonthermal electrons are repeatedly accelerated by periodic magnetic reconnections, which was predicted by the numerical simulation (Takasao & Shibata, 2016). However, the periodic magnetic reconnection is not detected directly due to the current instrumentation, that is, coronal magnetic fields can not be measured directly. The QPP feature observed in wavelengths of HXR and radio/microwave could be associated with accelerated electrons generated by quasi-periodic magnetic reconnections, such process has been discussed detailed in previous observations (Wu et al., 2016; D. Li, Ge, et al., 2021; Kumar et al., 2025). The 8-min QPP can also be interpreted by the periodic magnetic reconnection, since it is simultaneously observed in wavelengths of HXR, radio/microwave, Lyα, and white light. This feature also suggests that the nonthermal electrons may only precipitate into the lower chromosphere or the upper photosphere, where is the main source region of white-light emissions. Thus, the X4.0 flare belongs to 'Type I WLFs', as were categorized by Fang and Ding (1995). The 3-min period is simultaneously observed at the flare site and the nearby sunspot umbra, and they are connected by the closed magnetic field lines. So, it is possibly regarded as the leakage of sunspot oscillation in the form of slow MHD waves, which propagates from the sunspot umbra to the flare site along the closed magnetic loop, as shown in Figure 11 (a).

The coronal seismology aims to estimate the local plasma and magnetic properties using observed wave characteristics and their underlying mechanisms. According to

the MHD waves at kink (Nakariakov et al., 2021; Gao et al., 2024) and slow modes (Wang et al., 2021; Kolotkov, 2022), some plasma and magnetic properties in the corona can be estimated from Equations 1 and 2, respectively. In our case, both the 2-min and 8-min QPPs can be explained by the mechanism based upon a repetitive regime of magnetic reconnection, which might be modulated by the resonances of MHD waves. The 8-min QPP appears during the X4.0 flare, which shows a hot plasma loop (L1 $\approx$ 92 Mm), as indicated by the red arrow in Figure 4 (b2). The phase speed ($v_{\rm p}$) is estimated to about 400 km s^{-1}, which is less than the local sound speed ($v_{\rm s} \approx$ 480 km s^{-1}) in the solar corona at a high temperate (T) of about 10 MK. The polytropic (or effective adiabatic) index (α) can be estimated to about 1.16, consistent with that measured by Van Doorsselaere et al. (2011). By using the relation between $v_{\rm p}/v_{\rm s}$ and thermal ratio (d) given by Wang et al. (2021), the effective thermal ratio $d_{\rm e}$ could be estimated to about 0.18, the actual thermal ratio (d_0) is about 0.016, and the result of $d_{\rm e}/d_0$ is about 11.25 in the flare loop. All these facts suggest that the 8-min period is possibly modulated by the slow-mode wave. On the other hand, a hot plasma loop (L2 $\approx$ 63 Mm) is seen during the pre-flare phase (Figure 7 c). The phase speed is about 1050 km s^{-1}, which is in the range of kink speeds (Nakariakov & Kolotkov, 2020; Nakariakov et al., 2021). Therefore, the 2-min period is likely to be modulated by the kink wave, and the local Alfvén speed ($v_{\rm A}$) and magnetic field strength (B) are estimated to about 750 km s^{-1} and 40 G in the hot plasma loop, agreeing with our previous measurements in flare loops (D. Li et al., 2017, 2018). It should be pointed out that all those estimations are in the corona, i.e., hot plasma loops. The plasma and magnetic properties in lower atmospheres are difficult to be measured, largely due to their complex magnetic fields and high densities.

$$v_{\rm p} = \frac{2L}{P}, \quad v_{\rm A} = v_{\rm p}\,\sqrt{\frac{1+r_\rho}{2}}, \quad B \approx v_{\rm A}\,\sqrt{\mu_0\,\rho}. \tag{1}$$

Where, r_ρ is the density ratio between external and internal flare loop, μ_0 is the magnetic permittivity in vacuum, and ρ is the density of hot loop.

$$v_{\rm s} \approx 152\,\sqrt{T({\rm MK})}, \quad v_{\rm p} \approx \sqrt{\frac{\alpha}{\gamma}}\,v_{\rm s}, \quad d_0 = 4.93\,(\frac{T^{3/2}}{n\,P}). \tag{2}$$

Here, γ is the adiabatic index, and n is the number density of flare loop. T(MK) refers to that the loop temperature in the unit of MK.

The flare QPPs at periods of 3 and 8 minutes are both associated with slow-mode waves, but their generation mechanisms are clearly different. In the coronal environment, large-amplitude QPPs (i.e., >20%) could be triggered by slow magnetoacoustic waves when the duration of the heat pulse ($\triangle t_{\rm H}$) is shorter than the loop sound crossing time ($\tau_{\rm s}$) (Reale et al., 2019; Wang et al., 2021), as shown in Equation 3. In our case, $\tau_{\rm s}$ can be estimated to about 460 s at the X4.0 flare maximum. Under the assumption of $\triangle t_{\rm H} \simeq P$, the 3-min QPP may be directly modulated by the slow magnetoacoustic wave leaking from sunspot umbrae, as is illuminated in Figure 11 (a). Conversely, the 8-min QPP is generated by the repetitive magnetic reconnection that is triggered by the slow-mode wave in the solar corona, that is, the periodicity of magnetic reconnection is modulated by the slow-mode wave at a period of about 8 minutes, as shown in Figure 11 (b). Similarly, the 2-min QPP is generated by the periodic magnetic reconnections that is triggered by the kink wave.

$$\triangle t_{\rm H} < \tau_{\rm s} \sim 5\,\frac{L({\rm Mm})}{\sqrt{0.1\,T({\rm MK})}}. \tag{3}$$

In order to compare with the statistically established scaling laws for flare QPPs (Hayes et al., 2020), we perform the scaling law between the QPP period (P) and the flare duration (τ) with the relationship described in Equation 4. τ is determined by the

time interval of the start and stop times of the X4.0 flare that was defined in the GOES catalog, and it is 2760 s. C is a constant, which is about 0.5 given by Hayes et al. (2020). Then, the QPP period is estimated to be (1.68±0.01) minutes, which is clearly different from the multiple periods detected in this study. This is mainly because that the scaling laws presented by Hayes et al. (2020) only searched for periodicity in the timescale of 6−300 s in the GOES SXR channel, but the multiple periods in this study are found in a wide range of wavelengths. Therefore, the scaling laws for flare QPPs should be updated if we considering a wide wavelength range and a longer period range.

$$P \approx C\tau^{0.67\pm0.03}. \tag{4}$$

5 Summary

Based on the combined solar telescopes, i.e., ASO-S/HXI, ASO-S/LST, SDO/AIA, SDO/HMI, SDO/EVE, NVST, CHASE, SUTRI, GECAM, STIX, LYRA, GOES, CBS, DART, SWAVES, and NoRP, we explored flare QPPs at five quasi-periods in multiple wavebands, we also tried to explore their generation mechanisms. The main conclusions are summarized as follows:

1. The multi-periodic pulsations are detected during an X4.0 flare in various wavebands, i.e., at least five periods. The X4.0 flare could be regarded as a WLF, as it is simultaneously brightening in wavebands of WST 3600 Å, HMI continuum near 6173 Å, and NVST TiO 7058 Å. It belongs to the 'Type I WLFs'. This is the first report of the flare QPP that is seen in the channel of TiO 7058 Å.
2. A quasi-period at about 2 minutes is observed in HXR and radio (i.e., centimeter and decimeter) emissions during the flare precursor, which might be associated with the periodic magnetic reconnection, and it could be regarded as a precursory indicator of the powerful flare.
3. A quasi-period at about 3 minutes is simultaneously detected in channels of HXR, radio, and EUV/UV at double ribbons or footpoints. It is independent of temperature and could be directly modulated by the slow magnetoacoustic wave leaking from sunspot umbrae.
4. A quasi-period at about 8 minutes is simultaneously detected in wavebands of HXR, radio, EUV/UV, white light and Lyα during the X4.0 flare. It is probably triggered by quasi-periodic regimes of magnetic reconnection, which can periodically accelerate nonthermal electrons.
5. A quasi-period at about 14 minutes is found in wavelengths of SXR and high-temperature EUV from the precursor to the X4.0 flare. It depends on temperature and might be associated with the temperature fluctuation caused by loop-loop interaction.
6. A quasi-period at about 18 minutes is seen in STIX 4-10 keV. It could be regarded as three successive and repeated energy-release processes in different flare regions.

Open Research Section

Publicly available data sets were analyzed in this study. They can be found here: http://aso-s.pmo.ac.cn/sodc/dataArchive.jsp, https://sun10.bao.ac.cn/SUTRI/, https://ssdc.nju.edu.cn/NdchaseSatellite, http://jsoc.stanford.edu/, http://www.solarmonitor.org/.

Acknowledgments
This work is funded by the National Key R&D Program of China 2021YFA1600502 (2021YFA1600500), and 2022YFF0503002 (2022YFF0503000). This work is also supported by the Strategic Priority Research Program of the Chinese Academy of Sciences, Grant No. XDB0560000,

NSFC under grants 12473059. D. Li is also supported by the Specialized Research Fund for State Key Laboratories. We acknowledge the use of data from the Chinese MeridianProject. ASO-S mission is supported by the Strategic Priority Research Program on Space Science, the Chinese Academy of Sciences, Grant No. XDA15320000. SUTRI is a collaborative project conducted by the National Astronomical Observatories of CAS, Peking University, Tongji University, Xi'an Institute of Optics and Precision Mechanics of CAS and the Innovation Academy for Microsatellites of CAS. The CHASE mission is supported by China National Space Administration (CNSA). CBS consists of four subsystems is operated by SDU. DART is an interferometric imaging telescope supported by Chinese initiative Meridian Project phase 2. SDO is NASA's first mission in the Living with a Star program. The STIX instrument is an international collaboration between Switzerland, Poland, France, Czech Republic, Germany, Austria, Ireland, and Italy.

References

Andries, J., Arregui, I., & Goossens, M. (2005, May). Determination of the Coronal Density Stratification from the Observation of Harmonic Coronal Loop Oscillations. *Astrophys. J. Lett.*, *624*(1), L57-L60. doi: 10.1086/430347

Bai, X., Tian, H., Deng, Y., Wang, Z., Yang, J., Zhang, X., ... Zhang, Z. (2023, June). The Solar Upper Transition Region Imager (SUTRI) Onboard the SATech-01 Satellite. *Research in Astronomy and Astrophysics*, *23*(6), 065014. doi: 10.1088/1674-4527/accc74

Benz, A. O. (2017, December). Flare Observations. *Living Reviews in Solar Physics*, *14*(1), 2. doi: 10.1007/s41116-016-0004-3

Broomhall, A.-M., Davenport, J. R. A., Hayes, L. A., Inglis, A. R., Kolotkov, D. Y., McLaughlin, J. A., ... Van Doorsselaere, T. (2019, October). A Blueprint of State-of-the-art Techniques for Detecting Quasi-periodic Pulsations in Solar and Stellar Flares. *Astrophys. J. Suppl.*, *244*(2), 44. doi: 10.3847/1538-4365/ab40b3

Chelpanov, A., & Kobanov, N. (2021, December). Using Flare-Induced Modulation of Three- and Five-Minute Oscillations for Studying Wave Propagation in the Solar Atmosphere. *Sol. Phys.*, *296*(12), 180. doi: 10.1007/s11207-021-01910-5

Chen, X., Yan, Y., Tan, B., Huang, J., Wang, W., Chen, L., ... Masuda, S. (2019, June). Quasi-periodic Pulsations before and during a Solar Flare in AR 12242. *Astrophys. J.*, *878*(2), 78. doi: 10.3847/1538-4357/ab1d64

Chen, Y., Wu, Z., Liu, W., Schwartz, R. A., Zhao, D., Wang, B., & Du, G. (2017, July). Double-coronal X-Ray and Microwave Sources Associated with a Magnetic Breakout Solar Eruption. *Astrophys. J.*, *843*(1), 8. doi: 10.3847/1538-4357/aa7462

Chowdhury, P., Srivastava, A. K., Dwivedi, B. N., Sych, R., & Moon, Y. J. (2015, December). Study of multi-periodic coronal pulsations during an X-class solar flare. *Advances in Space Research*, *56*(12), 2769-2778. doi: 10.1016/j.asr.2015.08.003

Collier, H., Hayes, L. A., Yu, S., Battaglia, A. F., Ashfield, W., Polito, V., ... Krucker, S. (2024, April). Localising pulsations in the hard X-ray and microwave emission of an X-class flare. *Astron. Astrophys.*, *684*, A215. doi: 10.1051/0004-6361/202348652

Comisso, L. (2024, September). Concurrent Particle Acceleration and Pitch-angle Anisotropy Driven by Magnetic Reconnection: Ion-electron Plasmas. *Astrophys. J.*, *972*(1), 9. doi: 10.3847/1538-4357/ad51fe

Dominique, M., Hochedez, J. F., Schmutz, W., Dammasch, I. E., Shapiro, A. I., Kretzschmar, M., ... BenMoussa, A. (2013, August). The LYRA Instrument Onboard PROBA2: Description and In-Flight Performance. *Sol. Phys.*, *286*(1), 21-42. doi: 10.1007/s11207-013-0252-5

Fang, C., & Ding, M. D. (1995, April). On the spectral characteristics and atmo-

spheric models of two types of white-light flares. *Astron. Astrophys. Suppl.*, *110*, 99.

Feng, L., Li, H., Chen, B., Li, Y., Susino, R., Huang, Y., ... Zhang, Y. (2019, November). The Lyman-alpha Solar Telescope (LST) for the ASO-S mission - III. data and potential diagnostics. *Research in Astronomy and Astrophysics*, *19*(11), 162. doi: 10.1088/1674-4527/19/11/162

Feng, S., Deng, Z., Yuan, D., Xu, Z., & Yang, X. (2020, August). Propagating slow sausage waves in a sunspot observed by the New Vacuum Solar Telescope. *Research in Astronomy and Astrophysics*, *20*(8), 117. doi: 10.1088/1674-4527/20/8/117

Fleishman, G. D., Gary, D. E., Chen, B., Kuroda, N., Yu, S., & Nita, G. M. (2020, January). Decay of the coronal magnetic field can release sufficient energy to power a solar flare. *Science*, *367*(6475), 278-280. doi: 10.1126/science.aax6874

Fremstad, D., Guevara Gómez, J. C., Hudson, H., & Martínez Oliveros, J. C. (2023, April). An overview of HMI off-disk flare observations. *Astron. Astrophys.*, *672*, A32. doi: 10.1051/0004-6361/202245788

Gan, W.-Q., Zhu, C., Deng, Y.-Y., Li, H., Su, Y., Zhang, H.-Y., ... Tang, X.-J. (2019, November). Advanced Space-based Solar Observatory (ASO-S): an overview. *Research in Astronomy and Astrophysics*, *19*(11), 156. doi: 10.1088/1674-4527/19/11/156

Gao, Y., Van Doorsselaere, T., Tian, H., Guo, M., & Karampelas, K. (2024, September). Propagating kink waves in an open coronal magnetic flux tube with gravitational stratification: Magnetohydrodynamic simulation and forward modelling. *Astron. Astrophys.*, *689*, A195. doi: 10.1051/0004-6361/202450769

Gary, D. E., Chen, B., Dennis, B. R., Fleishman, G. D., Hurford, G. J., Krucker, S., ... Yu, S. (2018, August). Microwave and Hard X-Ray Observations of the 2017 September 10 Solar Limb Flare. *Astrophys. J.*, *863*(1), 83. doi: 10.3847/1538-4357/aad0ef

Hayes, L. A., Gallagher, P. T., Dennis, B. R., Ireland, J., Inglis, A. R., & Ryan, D. F. (2016, August). Quasi-periodic Pulsations during the Impulsive and Decay phases of an X-class Flare. *Astrophys. J. Lett.*, *827*(2), L30. doi: 10.3847/2041-8205/827/2/L30

Hayes, L. A., Inglis, A. R., Christe, S., Dennis, B., & Gallagher, P. T. (2020, May). Statistical Study of GOES X-Ray Quasi-periodic Pulsations in Solar Flares. *Astrophys. J.*, *895*(1), 50. doi: 10.3847/1538-4357/ab8d40

Horne, J. H., & Baliunas, S. L. (1986, March). A Prescription for Period Analysis of Unevenly Sampled Time Series. *Astrophys. J.*, *302*, 757. doi: 10.1086/164037

Howard, W. S., & MacGregor, M. A. (2022, February). No Such Thing as a Simple Flare: Substructure and Quasi-periodic Pulsations Observed in a Statistical Sample of 20 s Cadence TESS Flares. *Astrophys. J.*, *926*(2), 204. doi: 10.3847/1538-4357/ac426e

Huang, J., Tan, B., Zhang, Y., Zhu, X., Yang, S., & Deng, Y. (2024, April). The Slipping Magnetic Reconnection and Damped Quasiperiodic Pulsations in a Circular Ribbon Flare. *Astrophys. J.*, *965*(2), 137. doi: 10.3847/1538-4357/ad3353

Huang, Y., Li, H., Gan, W.-Q., Li, Y.-P., Su, J.-T., Deng, Y.-Y., ... Li, J.-W. (2019, November). The Science Operations and Data Center (SODC) of the ASO-S mission. *Research in Astronomy and Astrophysics*, *19*(11), 164. doi: 10.1088/1674-4527/19/11/164

Inglis, A., Hayes, L., Guidoni, S., McLaughlin, J., Nakariakov, V., Van Doorsselaere, T., ... Chen, T. (2023, July). Quasi-periodic pulsations in solar flares: a key diagnostic of energy release on the Sun. In *Bulletin of the american astronomical society* (Vol. 55, p. 181). doi: 10.3847/25c2cfeb.55d6b861

Inglis, A. R., & Dennis, B. R. (2012, April). The Relationship between Hard X-Ray

Pulse Timings and the Locations of Footpoint Sources during Solar Flares. *Astrophys. J.*, *748*(2), 139. doi: 10.1088/0004-637X/748/2/139

Inglis, A. R., & Hayes, L. A. (2024, August). Searching for Rapid Pulsations in Solar Flare X-Ray Data. *Astrophys. J.*, *971*(1), 29. doi: 10.3847/1538-4357/ad54bb

Inglis, A. R., Nakariakov, V. M., & Melnikov, V. F. (2008, September). Multi-wavelength spatially resolved analysis of quasi-periodic pulsations in a solar flare. *Astron. Astrophys.*, *487*(3), 1147-1153. doi: 10.1051/0004-6361:20079323

Joshi, R., Schmieder, B., Heinzel, P., Tomin, J., Chandra, R., & Vilmer, N. (2021, October). Balmer continuum enhancement detected in a mini flare observed with IRIS. *Astron. Astrophys.*, *654*, A31. doi: 10.1051/0004-6361/202141172

Kaiser, M. L., Kucera, T. A., Davila, J. M., St. Cyr, O. C., Guhathakurta, M., & Christian, E. (2008, April). The STEREO Mission: An Introduction. *Space Sci. Rev.*, *136*(1-4), 5-16. doi: 10.1007/s11214-007-9277-0

Karampelas, K., McLaughlin, J. A., Botha, G. J. J., & Régnier, S. (2023, February). Oscillatory Reconnection as a Plasma Diagnostic in the Solar Corona. *Astrophys. J.*, *943*(2), 131. doi: 10.3847/1538-4357/acac90

Karlický, M., & Rybák, J. (2020, October). The 2017 September 6 Flare: Radio Bursts and Pulsations in the 22-5000 MHz Range and Associated Phenomena. *Astrophys. J. Suppl.*, *250*(2), 31. doi: 10.3847/1538-4365/abb19f

Karlický, M., & Rybák, J. (2023, February). Multi-Periodicity of High-Frequency Type III Bursts as a Signature of the Fragmented Magnetic Reconnection. *Universe*, *9*(2), 92. doi: 10.3390/universe9020092

Kashapova, L. K., Kupriyanova, E. G., Xu, Z., Reid, H. A. S., & Kolotkov, D. Y. (2020, October). The origin of quasi-periodicities during circular ribbon flares. *Astron. Astrophys.*, *642*, A195. doi: 10.1051/0004-6361/201833947

Kolotkov, D. Y. (2022, December). Coronal seismology by slow waves in non-adiabatic conditions. *Frontiers in Astronomy and Space Sciences*, *9*, 402. doi: 10.3389/fspas.2022.1073664

Kolotkov, D. Y., Nakariakov, V. M., Holt, R., & Kuznetsov, A. A. (2021, December). Multiwavelength Quasi-periodic Pulsations in a Stellar Superflare. *Astrophys. J. Lett.*, *923*(2), L33. doi: 10.3847/2041-8213/ac432e

Kowalski, A. F. (2024, December). Stellar flares. *Living Reviews in Solar Physics*, *21*(1), 1. doi: 10.1007/s41116-024-00039-4

Krucker, S., Hurford, G. J., Grimm, O., Kögl, S., Gröbelbauer, H. P., Etesi, L., ... Lin, R. P. (2020, October). The Spectrometer/Telescope for Imaging X-rays (STIX). *Astron. Astrophys.*, *642*, A15. doi: 10.1051/0004-6361/201937362

Kumar, P., Karpen, J. T., & Dahlin, J. T. (2025, February). X-Ray/Radio Quasiperiodic Pulsations Associated with Plasmoids in Solar Flare Current Sheets. *Astrophys. J.*, *980*(2), 158. doi: 10.3847/1538-4357/ada293

Kumar, P., Nakariakov, V. M., & Cho, K.-S. (2016, May). Observation of a Quasiperiodic Pulsation in Hard X-Ray, Radio, and Extreme-ultraviolet Wavelengths. *Astrophys. J.*, *822*(1), 7. doi: 10.3847/0004-637X/822/1/7

Kumar, P., Nakariakov, V. M., Karpen, J. T., & Cho, K.-S. (2024, March). Direct imaging of magnetohydrodynamic wave mode conversion near a 3D null point on the sun. *Nature Communications*, *15*, 2667. doi: 10.1038/s41467-024-46736-4

Lemen, J. R., Title, A. M., Akin, D. J., Boerner, P. F., Chou, C., Drake, J. F., ... Waltham, N. (2012, January). The Atmospheric Imaging Assembly (AIA) on the Solar Dynamics Observatory (SDO). *Sol. Phys.*, *275*(1-2), 17-40. doi: 10.1007/s11207-011-9776-8

Li, C., Fang, C., Li, Z., Ding, M.-D., Chen, P.-F., Chen, Z., ... Zhang, W. (2019, November). Chinese Hα Solar Explorer (CHASE) - a complementary space mission to the ASO-S. *Research in Astronomy and Astrophysics*, *19*(11), 165. doi: 10.1088/1674-4527/19/11/165

Li, D. (2022, January). Quasi-periodic pulsations with double periods observed in Lyα emission during solar flares. *Science in China E: Technological Sciences*, *65*(1), 139-146. doi: 10.1007/s11431-020-1771-7

Li, D. (2025, March). Localizing short-period pulsations in hard X-rays and γ-rays during an X9.0 flare. *Astron. Astrophys.*, *695*, L4. doi: 10.1051/0004-6361/202453613

Li, D., & Chen, W. (2022, June). Quasi-periodic Accelerations of Energetic Particles during a Solar Flare. *Astrophys. J. Lett.*, *931*(2), L28. doi: 10.3847/2041-8213/ac6fd2

Li, D., Feng, S., Su, W., & Huang, Y. (2020, July). Preflare very long-periodic pulsations observed in Hα emission before the onset of a solar flare. *Astron. Astrophys.*, *639*, L5. doi: 10.1051/0004-6361/202038398

Li, D., Ge, M., Dominique, M., Zhao, H., Li, G., Li, X., ... Ning, Z. (2021, November). Detection of Flare Multiperiodic Pulsations in Mid-ultraviolet Balmer Continuum, Lyα, Hard X-Ray, and Radio Emissions Simultaneously. *Astrophys. J.*, *921*(2), 179. doi: 10.3847/1538-4357/ac1c05

Li, D., Hong, Z., Hou, Z., & Su, Y. (2024, July). Localizing Quasiperiodic Pulsations in Hard X-Ray, Microwave, and Lyα Emissions of an X6.4 Flare. *Astrophys. J.*, *970*(1), 77. doi: 10.3847/1538-4357/ad566c

Li, D., Li, J., Shen, J., Song, Q., Ji, H., & Ning, Z. (2024, October). Long-period energy releases during a C2.8 flare. *Astron. Astrophys.*, *690*, A39. doi: 10.1051/0004-6361/202450622

Li, D., Li, Z., Shi, F., Su, Y., Chen, W., Yu, F., ... Ning, Z. (2023, December). Observational signature of continuously operating drivers of decayless kink oscillation. *Astron. Astrophys.*, *680*, L15. doi: 10.1051/0004-6361/202348075

Li, D., Ning, Z. J., Huang, Y., Chen, N. H., Zhang, Q. M., Su, Y. N., & Su, W. (2017, November). Doppler Shift Oscillations from a Hot Line Observed by IRIS. *Astrophys. J.*, *849*(2), 113. doi: 10.3847/1538-4357/aa9073

Li, D., Wang, J., & Huang, Y. (2024, September). Very Long-periodic Pulsations Detected Simultaneously in a White-light Flare and Sunspot Penumbra. *Astrophys. J. Lett.*, *972*(1), L2. doi: 10.3847/2041-8213/ad6cde

Li, D., Warmuth, A., Lu, L., & Ning, Z. (2021, April). An investigation of flare emissions at multiple wavelengths. *Research in Astronomy and Astrophysics*, *21*(3), 066. doi: 10.1088/1674-4527/21/3/66

Li, D., Yuan, D., Su, Y. N., Zhang, Q. M., Su, W., & Ning, Z. J. (2018, September). Non-damping oscillations at flaring loops. *Astron. Astrophys.*, *617*, A86. doi: 10.1051/0004-6361/201832991

Li, D., & Zhang, Q. M. (2017, October). Quasi-periodic pulsations with multiple periods in hard X-ray emission. *Mon. Not. R. Astron. Soc.*, *471*(1), L6-L10. doi: 10.1093/mnrasl/slx091

Li, R., Zhao, X., Yan, J., Wu, L., Yang, Y., Lv, X., ... Liang, Y. (2024, February). Predicting the Arrival Time of an Interplanetary Shock Based on DSRT Spectrum Observations for the Corresponding Type II Radio Burst and a Blast Wave Theory. *Astrophys. J.*, *962*(2), 178. doi: 10.3847/1538-4357/ad150f

Li, T., Zhang, J., & Hou, Y. (2017, October). Flare Ribbons Approach Observed by the Interface Region Imaging Spectrograph and the Solar Dynamics Observatory. *Astrophys. J.*, *848*(1), 32. doi: 10.3847/1538-4357/aa8c01

Li, Y., Liu, X., Jing, Z., Chen, W., Li, Q., Su, Y., ... Gan, W. (2024, September). Various Features of the X-class White-light Flares in Super Active Region NOAA 13664. *Astrophys. J. Lett.*, *972*(1), L1. doi: 10.3847/2041-8213/ad6d6c

Lin, J., Soon, W., & Baliunas, S. L. (2003, April). Theories of solar eruptions: a review. *New Astronomy Reviews*, *47*(2), 53-84. doi: 10.1016/S1387-6473(02)00271-3

Liu, Z., Xu, J., Gu, B.-Z., Wang, S., You, J.-Q., Shen, L.-X., ... Zhang, B.-R.

(2014, June). New vacuum solar telescope and observations with high resolution. *Research in Astronomy and Astrophysics*, *14*(6), 705-718. doi: 10.1088/1674-4527/14/6/009

Lu, Z., Chen, F., Ding, M. D., Wang, C., Dai, Y., & Cheng, X. (2024, June). A model for heating the super-hot corona in solar active regions. *Nature Astronomy*, *8*, 706-715. doi: 10.1038/s41550-024-02244-5

Luo, Y., Chen, B., Yu, S., Battaglia, M., & Sharma, R. (2022, December). Multiple Regions of Nonthermal Quasiperiodic Pulsations during the Impulsive Phase of a Solar Flare. *Astrophys. J.*, *940*(2), 137. doi: 10.3847/1538-4357/ac997a

Masuda, S., Kosugi, T., Hara, H., Tsuneta, S., & Ogawara, Y. (1994, October). A loop-top hard X-ray source in a compact solar flare as evidence for magnetic reconnection. *Nature*, *371*(6497), 495-497. doi: 10.1038/371495a0

McLaughlin, J. A., Nakariakov, V. M., Dominique, M., Jelínek, P., & Takasao, S. (2018, February). Modelling Quasi-Periodic Pulsations in Solar and Stellar Flares. *Space Sci. Rev.*, *214*(1), 45. doi: 10.1007/s11214-018-0478-5

Mehta, T., Broomhall, A. M., & Hayes, L. A. (2023, August). Prevalence of non-stationarity in quasi-periodic pulsations (QPPs) associated with M- and X-class solar flares. *Mon. Not. R. Astron. Soc.*, *523*(3), 3689-3698. doi: 10.1093/mnras/stad1619

Millar, D. C. L., Fletcher, L., & Joshi, J. (2024, January). Intensity and velocity oscillations in a flaring active region. *Mon. Not. R. Astron. Soc.*, *527*(3), 5916-5928. doi: 10.1093/mnras/stad3386

Milligan, R. O., Fleck, B., Ireland, J., Fletcher, L., & Dennis, B. R. (2017, October). Detection of Three-minute Oscillations in Full-disk Lyα Emission during a Solar Flare. *Astrophys. J. Lett.*, *848*(1), L8. doi: 10.3847/2041-8213/aa8f3a

Nakariakov, V. M., Anfinogentov, S., Storozhenko, A. A., Kurochkin, E. A., Bogod, V. M., Sharykin, I. N., & Kaltman, T. I. (2018, June). Quasi-periodic Pulsations in a Solar Microflare. *Astrophys. J.*, *859*(2), 154. doi: 10.3847/1538-4357/aabfb9

Nakariakov, V. M., Anfinogentov, S. A., Antolin, P., Jain, R., Kolotkov, D. Y., Kupriyanova, E. G., ... Zimovets, I. V. (2021, September). Kink Oscillations of Coronal Loops. *Space Sci. Rev.*, *217*(6), 73. doi: 10.1007/s11214-021-00847-2

Nakariakov, V. M., & Kolotkov, D. Y. (2020, August). Magnetohydrodynamic Waves in the Solar Corona. *Annu. Rev. Astron. Astrophys.*, *58*, 441-481. doi: 10.1146/annurev-astro-032320-042940

Nakariakov, V. M., Kolotkov, D. Y., Kupriyanova, E. G., Mehta, T., Pugh, C. E., Lee, D. H., & Broomhall, A. M. (2019, January). Non-stationary quasi-periodic pulsations in solar and stellar flares. *Plasma Physics and Controlled Fusion*, *61*(1), 014024. doi: 10.1088/1361-6587/aad97c

Nakariakov, V. M., Pascoe, D. J., & Arber, T. D. (2005, November). Short Quasi-Periodic MHD Waves in Coronal Structures. *Space Sci. Rev.*, *121*(1-4), 115-125. doi: 10.1007/s11214-006-4718-8

Nakariakov, V. M., & Zimovets, I. V. (2011, April). Slow Magnetoacoustic Waves in Two-ribbon Flares. *Astrophys. J. Lett.*, *730*(2), L27. doi: 10.1088/2041-8205/730/2/L27

Priest, E. R., & Forbes, T. G. (2002, January). The magnetic nature of solar flares. *Astron. Astrophys. Rev.*, *10*(4), 313-377. doi: 10.1007/s001590100013

Pugh, C. E., Broomhall, A. M., & Nakariakov, V. M. (2019, April). Scaling laws of quasi-periodic pulsations in solar flares. *Astron. Astrophys.*, *624*, A65. doi: 10.1051/0004-6361/201834455

Reale, F., Testa, P., Petralia, A., & Kolotkov, D. Y. (2019, October). Large-amplitude Quasiperiodic Pulsations as Evidence of Impulsive Heating in Hot Transient Loop Systems Detected in the EUV with SDO/AIA. *Astrophys. J.*, *884*(2), 131. doi: 10.3847/1538-4357/ab4270

Reznikova, V. E., & Shibasaki, K. (2011, January). Flare quasi-periodic pulsations with growing periodicity. *Astron. Astrophys.*, *525*, A112. doi: 10.1051/0004-6361/201015600

Scargle, J. D. (1982, December). Studies in astronomical time series analysis. II. Statistical aspects of spectral analysis of unevenly spaced data. *Astrophys. J.*, *263*, 835-853. doi: 10.1086/160554

Schou, J., Scherrer, P. H., Bush, R. I., Wachter, R., Couvidat, S., Rabello-Soares, M. C., ... Tomczyk, S. (2012, January). Design and Ground Calibration of the Helioseismic and Magnetic Imager (HMI) Instrument on the Solar Dynamics Observatory (SDO). *Sol. Phys.*, *275*(1-2), 229-259. doi: 10.1007/s11207-011-9842-2

Schrijver, C. J., & De Rosa, M. L. (2003, January). Photospheric and heliospheric magnetic fields. *Sol. Phys.*, *212*(1), 165-200. doi: 10.1023/A:1022908504100

Shang, Z., Xu, K., Liu, Y., Wu, Z., Lu, G., Zhang, Y., ... Yan, F. (2022, February). A Broadband Solar Radio Dynamic Spectrometer Working in the Millimeter-wave Band. *Astrophys. J. Suppl.*, *258*(2), 25. doi: 10.3847/1538-4365/ac4257

Sharma, R., Battaglia, M., Yu, S., Chen, B., Luo, Y., & Krucker, S. (2024, July). Study of Particle Acceleration Using Fine Structures and Oscillations in Microwaves from the Electron Cyclotron Maser. *Astrophys. J.*, *970*(1), 17. doi: 10.3847/1538-4357/ad4884

Shen, Y., Zhou, X., Duan, Y., Tang, Z., Zhou, C., & Tan, S. (2022, February). Coronal Quasi-periodic Fast-mode Propagating Wave Trains. *Sol. Phys.*, *297*(2), 20. doi: 10.1007/s11207-022-01953-2

Shi, F., Li, D., Ning, Z., Warmuth, A., Chen, W., Su, Y., ... Yang, Y. (2024, March). Multiwavelength Observations of Quasiperiodic Pulsations in the Impulsive Phase of an Eruptive Flare with the Hard X-Ray Imager On Board ASO-S and Other Instruments. *Sol. Phys.*, *299*(3), 30. doi: 10.1007/s11207-024-02272-4

Shibata, K., & Magara, T. (2011, December). Solar Flares: Magnetohydrodynamic Processes. *Living Reviews in Solar Physics*, *8*(1), 6. doi: 10.12942/lrsp-2011-6

Shibayama, T., Maehara, H., Notsu, S., Notsu, Y., Nagao, T., Honda, S., ... Shibata, K. (2013, November). Superflares on Solar-type Stars Observed with Kepler. I. Statistical Properties of Superflares. *Astrophys. J. Suppl.*, *209*(1), 5. doi: 10.1088/0067-0049/209/1/5

Song, Y., Tian, H., Zhu, X., Chen, Y., Zhang, M., & Zhang, J. (2020, April). A White-light Flare Powered by Magnetic Reconnection in the Lower Solar Atmosphere. *Astrophys. J. Lett.*, *893*(1), L13. doi: 10.3847/2041-8213/ab83fa

Su, J. T., Liu, Y., Liu, S., Zhang, Y. Z., Zhao, H., Xu, H. Q., & Xie, W. B. (2013, January). Simultaneous Observation of Solar Oscillations Associated with Coronal Loops from the Photosphere to the Corona. *Astrophys. J.*, *762*(1), 42. doi: 10.1088/0004-637X/762/1/42

Su, Y., Liu, W., Li, Y.-P., Zhang, Z., Hurford, G. J., Chen, W., ... Gan, W.-Q. (2019, November). Simulations and software development for the Hard X-ray Imager onboard ASO-S. *Research in Astronomy and Astrophysics*, *19*(11), 163. doi: 10.1088/1674-4527/19/11/163

Sych, R., Nakariakov, V. M., Karlicky, M., & Anfinogentov, S. (2009, October). Relationship between wave processes in sunspots and quasi-periodic pulsations in active region flares. *Astron. Astrophys.*, *505*(2), 791-799. doi: 10.1051/0004-6361/200912132

Sych, R., Zhu, X., Chen, Y., & Yan, F. (2024, April). Spatial structure of resonance cavities in sunspots. *Mon. Not. R. Astron. Soc.*, *529*(2), 967-978. doi: 10.1093/mnras/stae575

Sych, R. A., & Nakariakov, V. M. (2008, April). The Pixelised Wavelet Filtering Method to Study Waves and Oscillations in Time Sequences of Solar Atmo-

spheric Images. *Sol. Phys.*, *248*(2), 395-408. doi: 10.1007/s11207-007-9005-7

Takasao, S., & Shibata, K. (2016, June). Above-the-loop-top Oscillation and Quasi-periodic Coronal Wave Generation in Solar Flares. *Astrophys. J.*, *823*(2), 150. doi: 10.3847/0004-637X/823/2/150

Tan, B., Yu, Z., Huang, J., Tan, C., & Zhang, Y. (2016, December). Very Long-period Pulsations before the Onset of Solar Flares. *Astrophys. J.*, *833*(2), 206. doi: 10.3847/1538-4357/833/2/206

Tan, B., Zhang, Y., Tan, C., & Liu, Y. (2010, November). Microwave Quasi-Periodic Pulsations in Multi-timescales Associated with a Solar Flare/CME Event. *Astrophys. J.*, *723*(1), 25-39. doi: 10.1088/0004-637X/723/1/25

Temmer, M., Veronig, A. M., Vršnak, B., & Miklenic, C. (2007, January). Energy Release Rates along Hα Flare Ribbons and the Location of Hard X-Ray Sources. *Astrophys. J.*, *654*(1), 665-674. doi: 10.1086/509634

Tian, H. (2017, October). Probing the solar transition region: current status and future perspectives. *Research in Astronomy and Astrophysics*, *17*(11), 110. doi: 10.1088/1674-4527/17/11/110

Tian, H., McIntosh, S. W., Wang, T., Ofman, L., De Pontieu, B., Innes, D. E., & Peter, H. (2012, November). Persistent Doppler Shift Oscillations Observed with Hinode/EIS in the Solar Corona: Spectroscopic Signatures of Alfvénic Waves and Recurring Upflows. *Astrophys. J.*, *759*(2), 144. doi: 10.1088/0004-637X/759/2/144

Tian, H., Young, P. R., Reeves, K. K., Wang, T., Antolin, P., Chen, B., & He, J. (2016, May). Global Sausage Oscillation of Solar Flare Loops Detected by the Interface Region Imaging Spectrograph. *Astrophys. J. Lett.*, *823*(1), L16. doi: 10.3847/2041-8205/823/1/L16

Torrence, C., & Compo, G. P. (1998, January). A Practical Guide to Wavelet Analysis. *Bulletin of the American Meteorological Society*, *79*(1), 61-78. doi: 10.1175/1520-0477(1998)079⟨0061:APGTWA⟩2.0.CO;2

Van Doorsselaere, T., Wardle, N., Del Zanna, G., Jansari, K., Verwichte, E., & Nakariakov, V. M. (2011, February). The First Measurement of the Adiabatic Index in the Solar Corona Using Time-dependent Spectroscopy of Hinode/EIS Observations. *Astrophys. J. Lett.*, *727*(2), L32. doi: 10.1088/2041-8205/727/2/L32

Verth, G., & Erdélyi, R. (2008, August). Effect of longitudinal magnetic and density inhomogeneity on transversal coronal loop oscillations. *Astron. Astrophys.*, *486*(3), 1015-1022. doi: 10.1051/0004-6361:200809626

Wang, T., Ofman, L., Yuan, D., Reale, F., Kolotkov, D. Y., & Srivastava, A. K. (2021, March). Slow-Mode Magnetoacoustic Waves in Coronal Loops. *Space Sci. Rev.*, *217*(2), 34. doi: 10.1007/s11214-021-00811-0

Warmuth, A., Önel, H., Mann, G., Rendtel, J., Strassmeier, K. G., Denker, C., ... Ber, K. (2020, July). The STIX Aspect System (SAS): The Optical Aspect System of the Spectrometer/Telescope for Imaging X-Rays (STIX) on Solar Orbiter. *Sol. Phys.*, *295*(7), 90. doi: 10.1007/s11207-020-01660-w

White, S. M., Thomas, R. J., & Schwartz, R. A. (2005, April). Updated Expressions for Determining Temperatures and Emission Measures from Goes Soft X-Ray Measurements. *Sol. Phys.*, *227*(2), 231-248. doi: 10.1007/s11207-005-2445-z

Woods, T. N., Eparvier, F. G., Hock, R., Jones, A. R., Woodraska, D., Judge, D., ... Viereck, R. (2012, January). Extreme Ultraviolet Variability Experiment (EVE) on the Solar Dynamics Observatory (SDO): Overview of Science Objectives, Instrument Design, Data Products, and Model Developments. *Sol. Phys.*, *275*(1-2), 115-143. doi: 10.1007/s11207-009-9487-6

Wu, Z., Chen, Y., Huang, G., Nakajima, H., Song, H., Melnikov, V., ... Jiao, F. (2016, April). Microwave Imaging of a Hot Flux Rope Structure during the Pre-impulsive Stage of an Eruptive M7.7 Solar Flare. *Astrophys. J. Lett.*, *820*(2), L29. doi: 10.3847/2041-8205/820/2/L29

Xiao, S., Liu, Y. Q., Peng, W. X., An, Z. H., Xiong, S. L., Tuo, Y. L., ... Zhang, S. N. (2022, March). On-ground and on-orbit time calibrations of GECAM. *Mon. Not. R. Astron. Soc.*, *511*(1), 964-971. doi: 10.1093/mnras/stac085

Yan, F., Wu, Z., Shang, Z., Wang, B., Zhang, L., & Chen, Y. (2023, January). The First Flare Observation with a New Solar Microwave Spectrometer Working in 35-40 GHz. *Astrophys. J. Lett.*, *942*(1), L11. doi: 10.3847/2041-8213/acad02

Yan, J., Wu, J., Wu, L., Yang, Y., Wu, J., Yan, Y., & Wang, C. (2023, June). A super radio camera with a one-kilometre lens. *Nature Astronomy*, *7*, 750-750. doi: 10.1038/s41550-023-01932-y

Yan, X., Liu, Z., Zhang, J., & Xu, Z. (2020, September). Research progress based on observations of the New Vacuum Solar Telescope. *Science in China E: Technological Sciences*, *63*(9), 1656-1674. doi: 10.1007/s11431-019-1463-6

Yan, X., Xue, Z., Jiang, C., Priest, E. R., Kliem, B., Yang, L., ... Liu, Z. (2022, February). Fast plasmoid-mediated reconnection in a solar flare. *Nature Communications*, *13*, 640. doi: 10.1038/s41467-022-28269-w

Yan, Y., He, H., Li, C., Esamdin, A., Tan, B. L., Zhang, L. Y., & Wang, H. (2021, July). Characteristic time of stellar flares on Sun-like stars. *Mon. Not. R. Astron. Soc.*, *505*(1), L79-L83. doi: 10.1093/mnrasl/slab055

Yuan, D. (2015, September). Signature of high-order azimuthal MHD body modes in sunspot's low atmosphere. *Research in Astronomy and Astrophysics*, *15*(9), 1449. doi: 10.1088/1674-4527/15/9/001

Yuan, D., Feng, S., Li, D., Ning, Z., & Tan, B. (2019, December). A Compact Source for Quasi-periodic Pulsation in an M-class Solar Flare. *Astrophys. J. Lett.*, *886*(2), L25. doi: 10.3847/2041-8213/ab5648

Yuan, D., Nakariakov, V. M., Chorley, N., & Foullon, C. (2011, September). Leakage of long-period oscillations from the chromosphere to the corona. *Astron. Astrophys.*, *533*, A116. doi: 10.1051/0004-6361/201116933

Yuan, D., Sych, R., Reznikova, V. E., & Nakariakov, V. M. (2014, January). Multi-height observations of magnetoacoustic cut-off frequency in a sunspot atmosphere. *Astron. Astrophys.*, *561*, A19. doi: 10.1051/0004-6361/201220208

Zhang, Q. (2024, March). Circular-ribbon flares and the related activities. *Reviews of Modern Plasma Physics*, *8*(1), 7. doi: 10.1007/s41614-024-00144-9

Zhang, Y., Li, T., & Ye, J. (2024, September). Quasiperiodic Oscillations of Flare Loops and Slipping Motion of Ribbon Substructures during a C-class Flare. *Astrophys. J.*, *972*(1), 122. doi: 10.3847/1538-4357/ad5e69

Zhao, J., Liu, W., & Vial, J.-C. (2021, November). White-light Continuum Observation of the Off-limb Loops of the SOL2017-09-10 X8.2 Flare: Temporal and Spatial Variations. *Astrophys. J. Lett.*, *921*(2), L26. doi: 10.3847/2041-8213/ac3339

Zhou, X., Shen, Y., Yuan, D., Keppens, R., Zhao, X., Fu, L., ... Zhou, C. (2024, April). Resolved magnetohydrodynamic wave lensing in the solar corona. *Nature Communications*, *15*, 3281. doi: 10.1038/s41467-024-46846-z

Zimovets, I. V., McLaughlin, J. A., Srivastava, A. K., Kolotkov, D. Y., Kuznetsov, A. A., Kupriyanova, E. G., ... Zhang, Q. M. (2021, August). Quasi-Periodic Pulsations in Solar and Stellar Flares: A Review of Underpinning Physical Mechanisms and Their Predicted Observational Signatures. *Space Sci. Rev.*, *217*(5), 66. doi: 10.1007/s11214-021-00840-9

Zimovets, I. V., Sharykin, I. N., Kaltman, T. I., Stupishin, A. G., & Nizamov, B. A. (2023, September). Preflare X-ray Pulsations with Sources Outside the Main Flare Active Region. *Geomagnetism and Aeronomy*, *63*(5), 513-526. doi: 10.1134/S0016793223600455

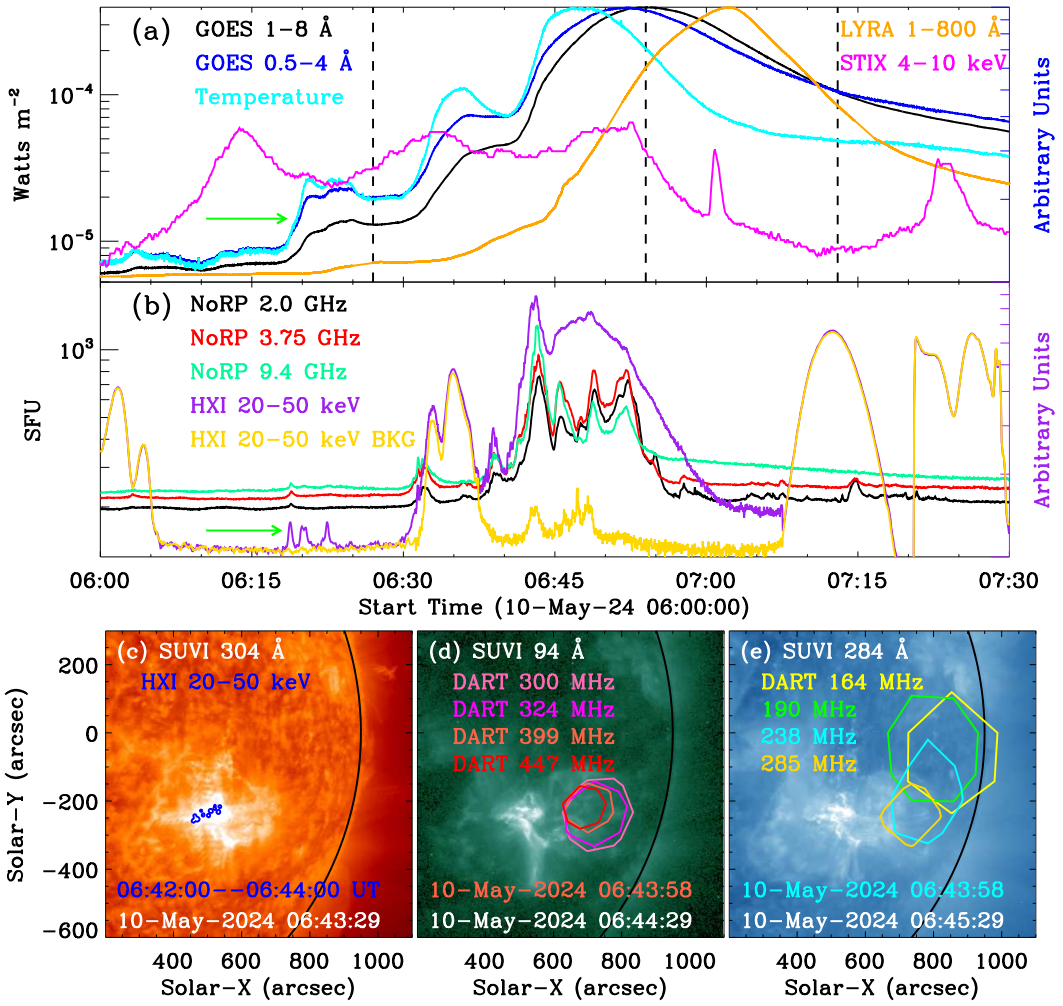

Figure 1. Overview of a powerful flare occurred on 2024 May 10. (a): Light curves measured by GOES 1-8 Å, 0.5-4 Å, and temperature, LYRA 1-800 Å, and STIX 4-10 keV. The vertical lines mark the start, peak and stop times of the powerful flare. (b): Time series recorded by NoRP 2.0 GHz, 3.75 GHz, and 9.4 GHz, HXI 20-50 keV and its background. The green arrow indicates a flare precursor. (c)-(e): EUV snapshots with a large FOV of $900'' \times 900''$ measured by GOES/SUVI in wavelengths of 304 Å, 94 Å, and 284 Å. The blue contours represent the flare radiation in the HXR channel, and the contour level is set at 10%. The colored contours in panels (d) and (e) outlines the radio radiation observed by DART, and their contour levels are set at 60%.

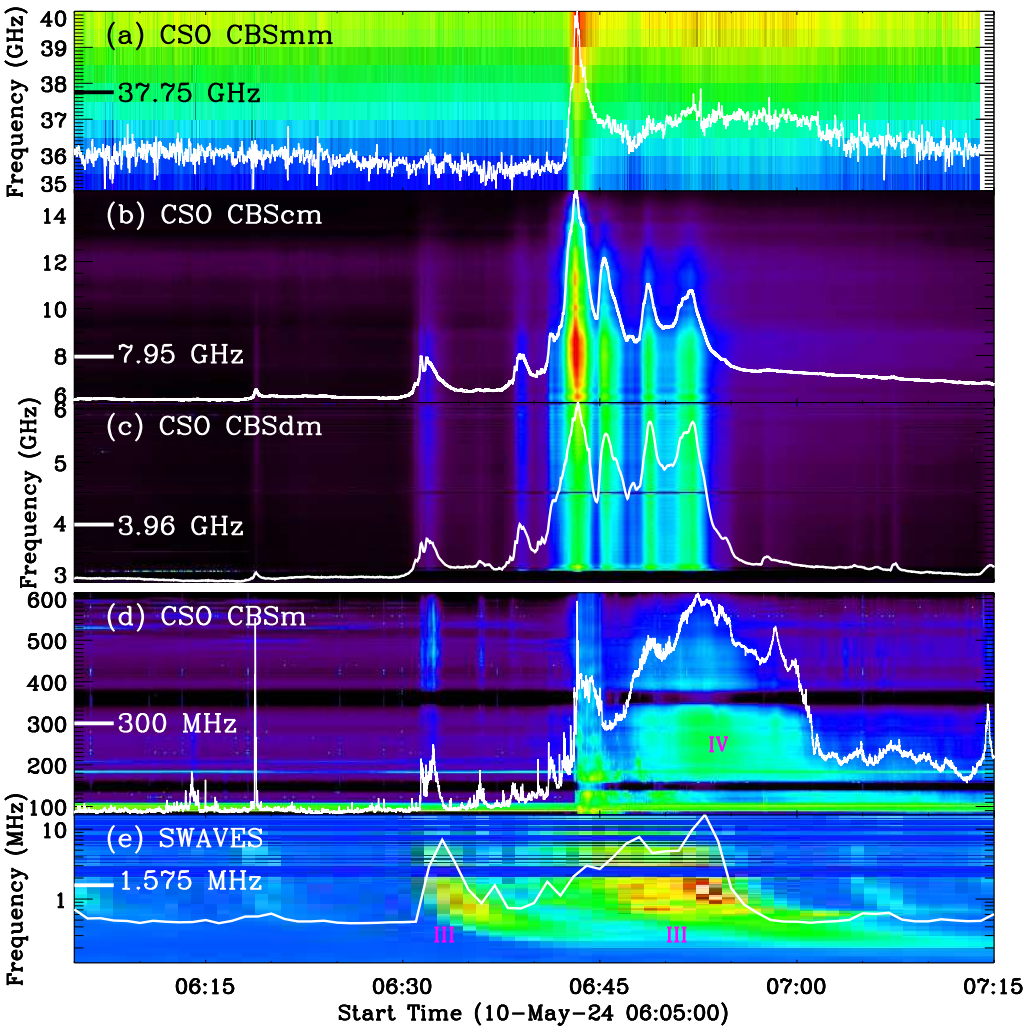

Figure 2. Dynamic radio spectra measured by CSO Radiaheliograph (millimeter, centimeter, decimeter, and meter-decameter regimes) and SWAVES. The overplotted curves are the radio fluxes derived from the radio spectra, as marked by the short line in each panel.

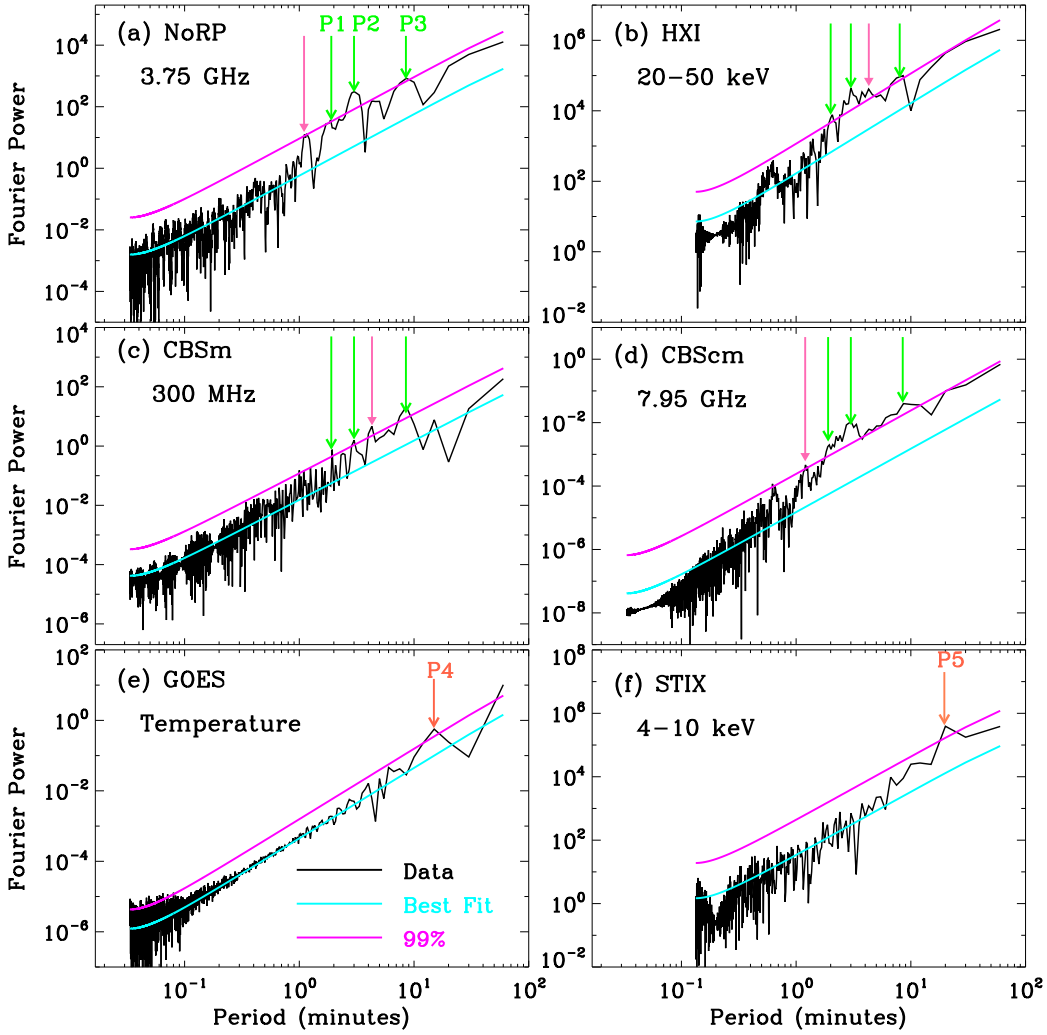

Figure 3. Fourier power spectra of raw light curves in multiple wavelengths. The cyan line in each panel represents a best-fit result for the observational data (black), and the magenta line indicates the confidence level at 99%. The color arrows mark quasi-periods for P1-P5 above the confidence level.

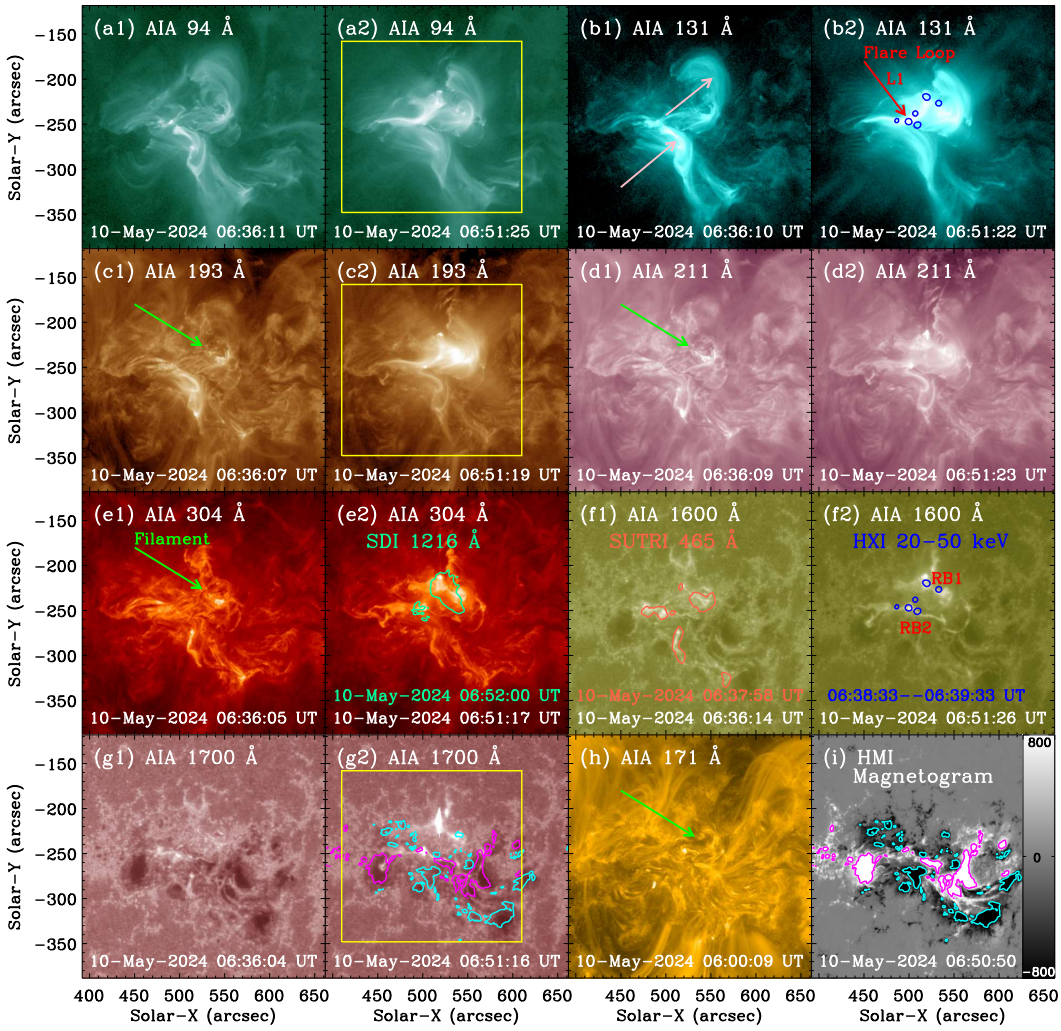

Figure 4. (a1)-(g2): EUV/UV snapshots captured by SDO/AIA at ∼06:36 UT and ∼06:51 UT during the X4.0 flare. (h): The AIA 171 Å map at about 06:00 UT before the X4.0 flare. (i): The LOS magnetogram measured by SDO/HMI. They have a same FOV of about 270″×270″. The blue contours represent the HXR emission at HXI 20-50 keV, and the level is set at 50%. The magenta and cyan contours are the positive and negative magnetic fields at a strength of ±800 G. The pink and red arrow marks the hot flare loop, and the green arrow indicates a filament. The yellow rectangle outlines the flare area used to integrate the intensity curve observed by SDO/AIA and ASO-S/SDI.

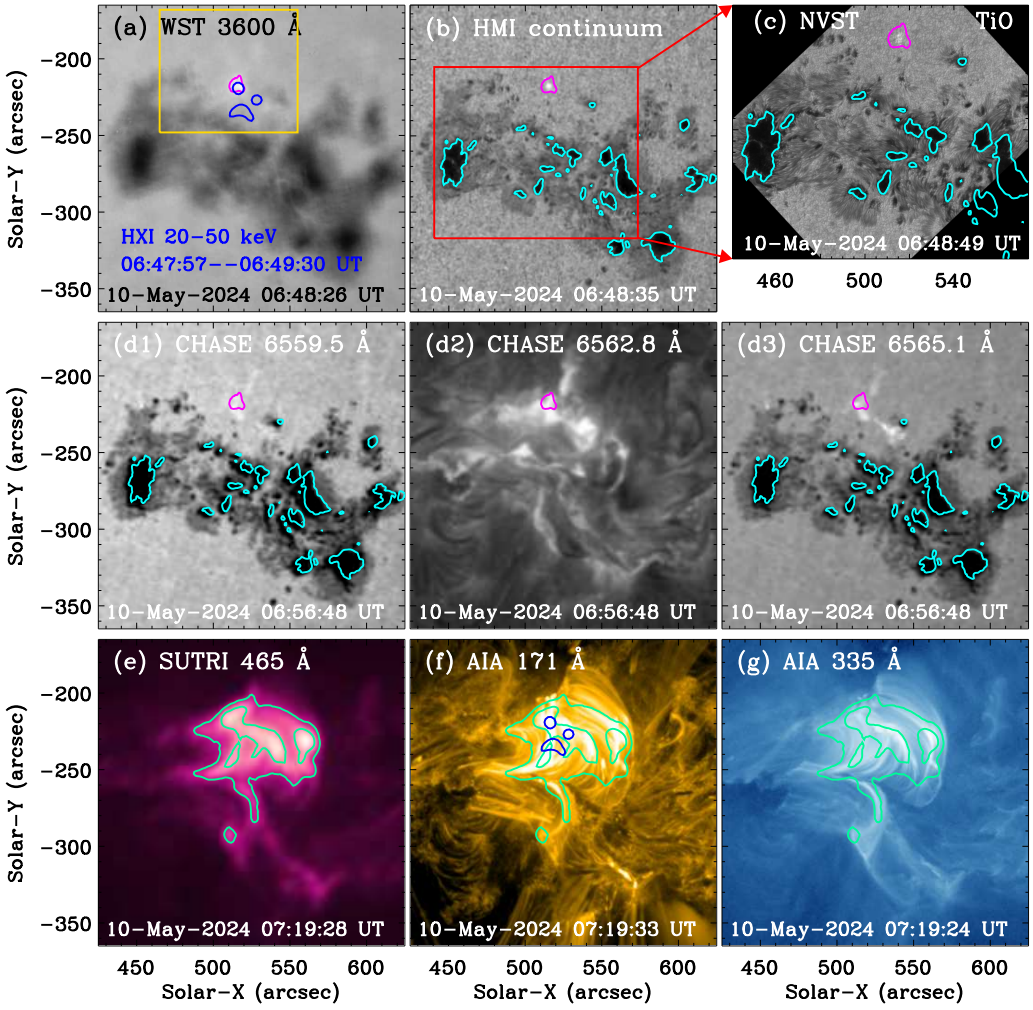

Figure 5. Multi-wavelength snapshots measured by ASO-S/WST, SDO/HMI, NVST, CHASE, SUTRI, and SDO/AIA. They have a small FOV of about 200″×200″, and the TiO-band map has a much smaller FOV of 133″×112″ due to the observational limit, as outlined by the red rectangle in panel (b). The magenta contour outlines the white-light brightening in the wavelength of WST 3600 Å, and the blue contours represent HXR emissions in the channel of HXI 20-50 keV at levels of 50%. The cyan contours outline the sunspot umbra, and the spring green contours outline the post flare loops. The gold rectangle outlines the flare area used to integrate the white-light flux.

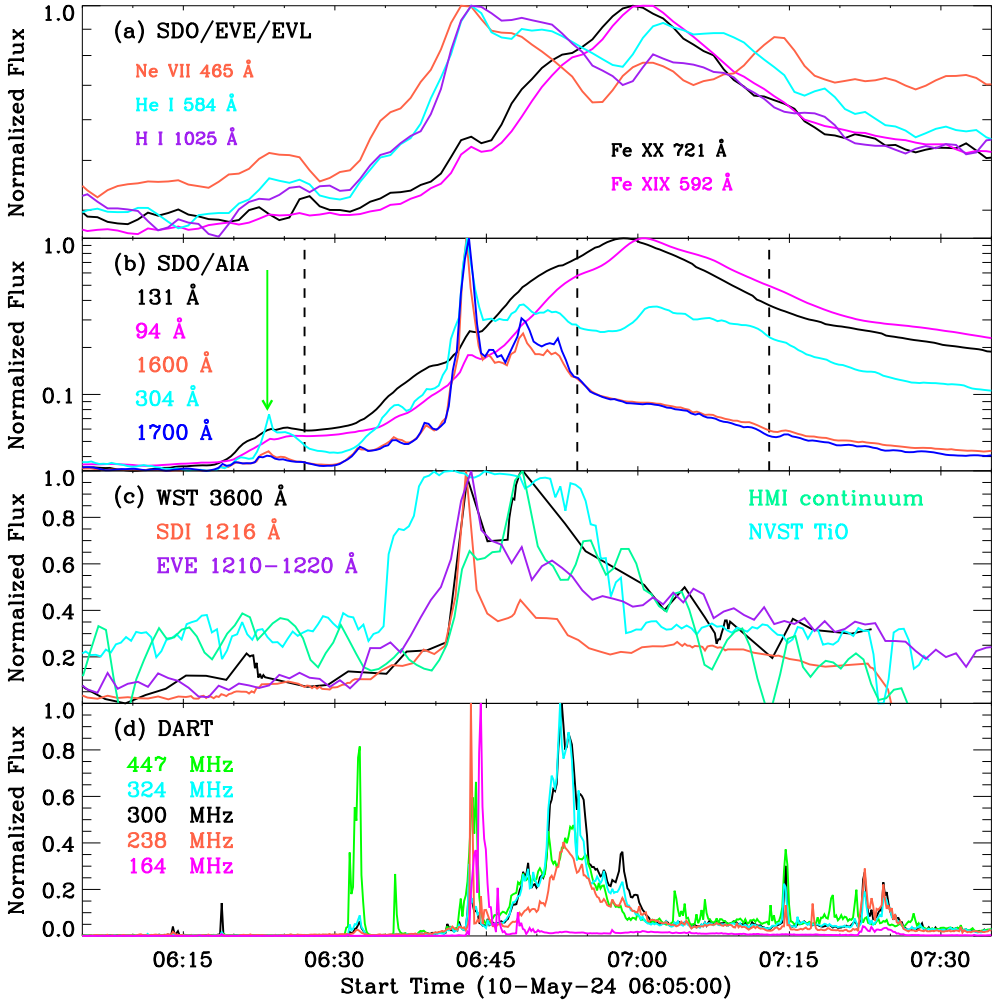

Figure 6. Multi-wavelength light curves. (a): Full-disk light curves recorded by SDO/EVE for the isolated lines. (b): Local intensity curves integrated over the flare area measured by SDO/AIA. The green arrow indicates the flare precursor. (c): Local time series integrated over the flare region observed by WST, SDI, HMI, and NVST, and the full-disk Lyα flux recorded by SDO/EVE. (d) Local light curves in radio emissions integrated over the active region measured by DART.

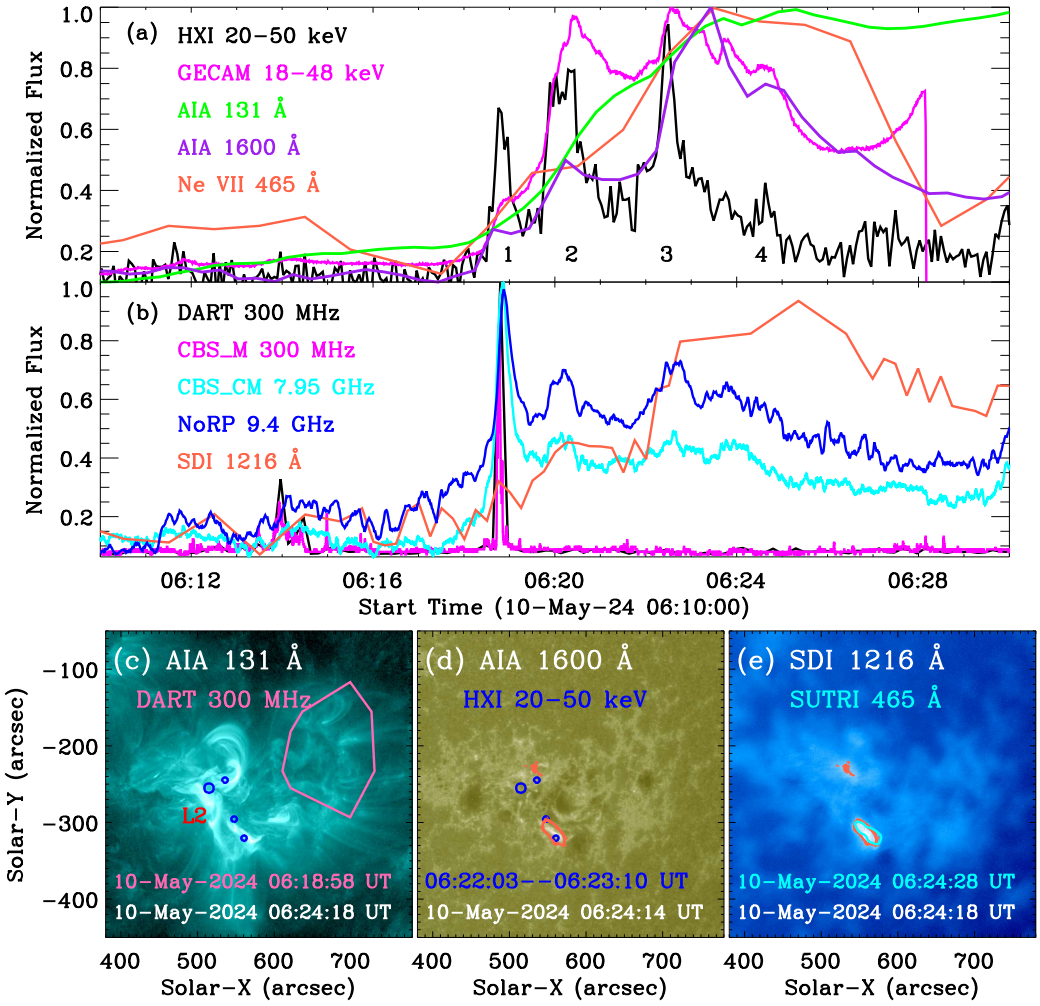

Figure 7. Overview of the pre-flare phase. (a) and (b): Multi-wavelength light curves measured by HXI, GECAM, SDO/AIA, SDO/EVE, DART, CBS, NoRP, and SDI. (c): Multi-wavelength maps observed by SDO/AIA and LST/SDI. The overlaid contours outline the flare radiation measured by HXI 20-50 keV (blue, 10% level), DART 300 MHz (hot pink, 80% level), SDI 1216 Å (tomato), and SUTRI 465 Å (cyan).

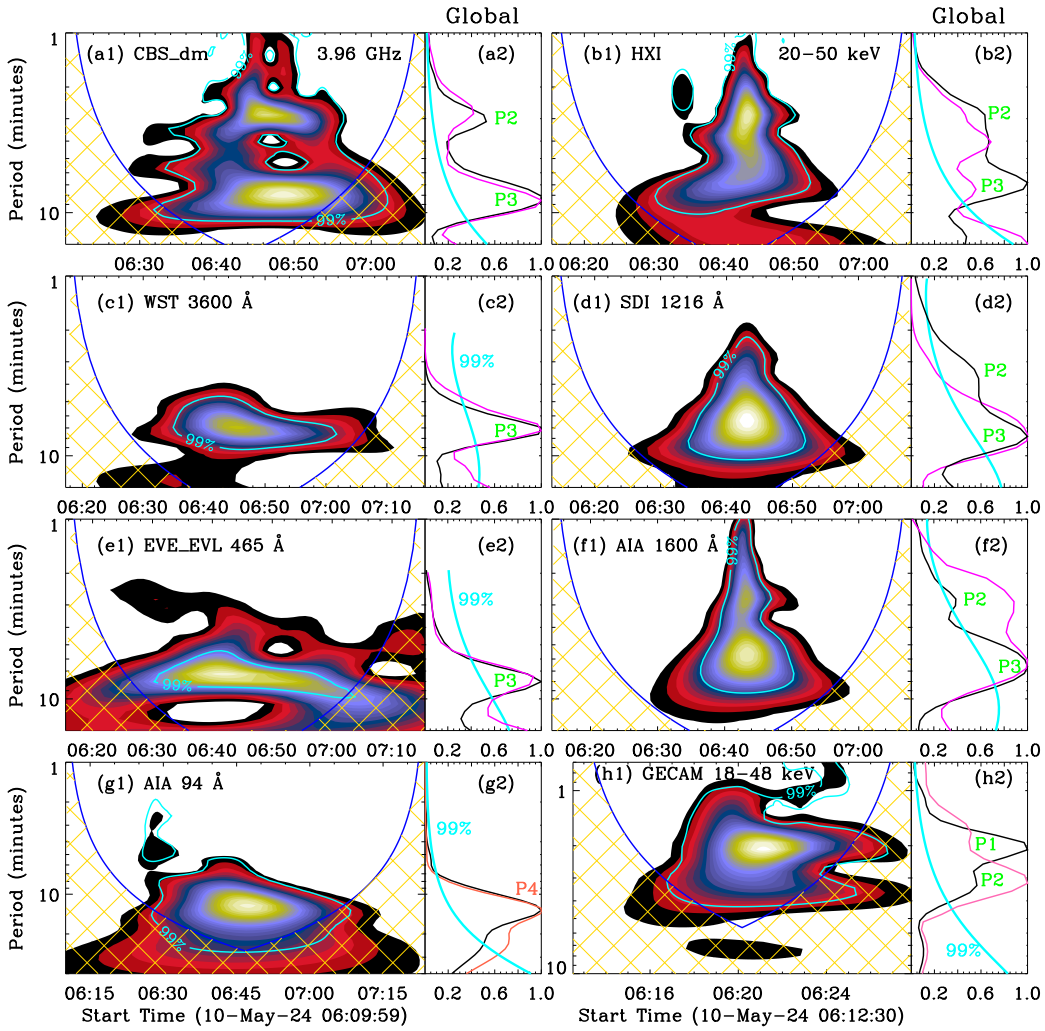

Figure 8. Morlet wavelet analysis results. (a1)-(h1): Morlet wavelet power spectra. (a2)-(f2): Global wavelet power spectra for the running windows of 10 minutes (black) and 15 minutes (magenta), respectively. (g2): Global wavelet power spectra for the running windows of 15 minutes (black) and 20 minutes (tomato). (h2): Global wavelet power spectra for the running windows of 3 minutes (black) and 5 minutes (hot pink). The cyan contours and lines represent the significance level of 99%.

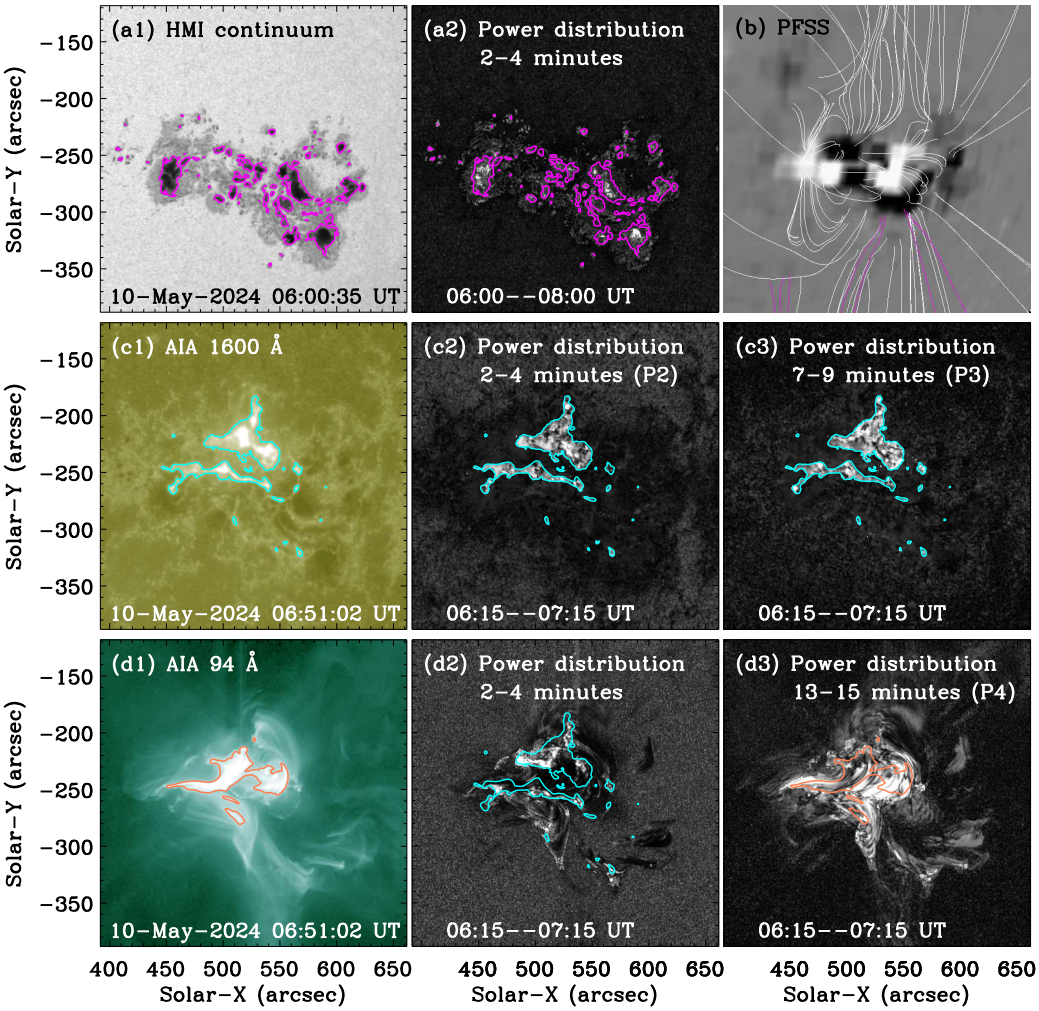

Figure 9. (a1)-(d1): Multi-wavelengths images in wavelengths of HMI continuum, AIA 1600 Å, and 94 Å. The overlaid contours outline the sunspot umbras (magenta), double flare ribbons (cyan) and hot flare loops (tomato), respectively. (b): The magnetic field lines extrapolated from a PFSS model. The purple and white lines indicate the open and closed magnetic fields, respectively. (a2)-(d3): Fourier power maps that are averaged over 2-4 minutes (a2-d2) and 7-10 minutes (c3) or 13-15 minutes (d3), respectively.

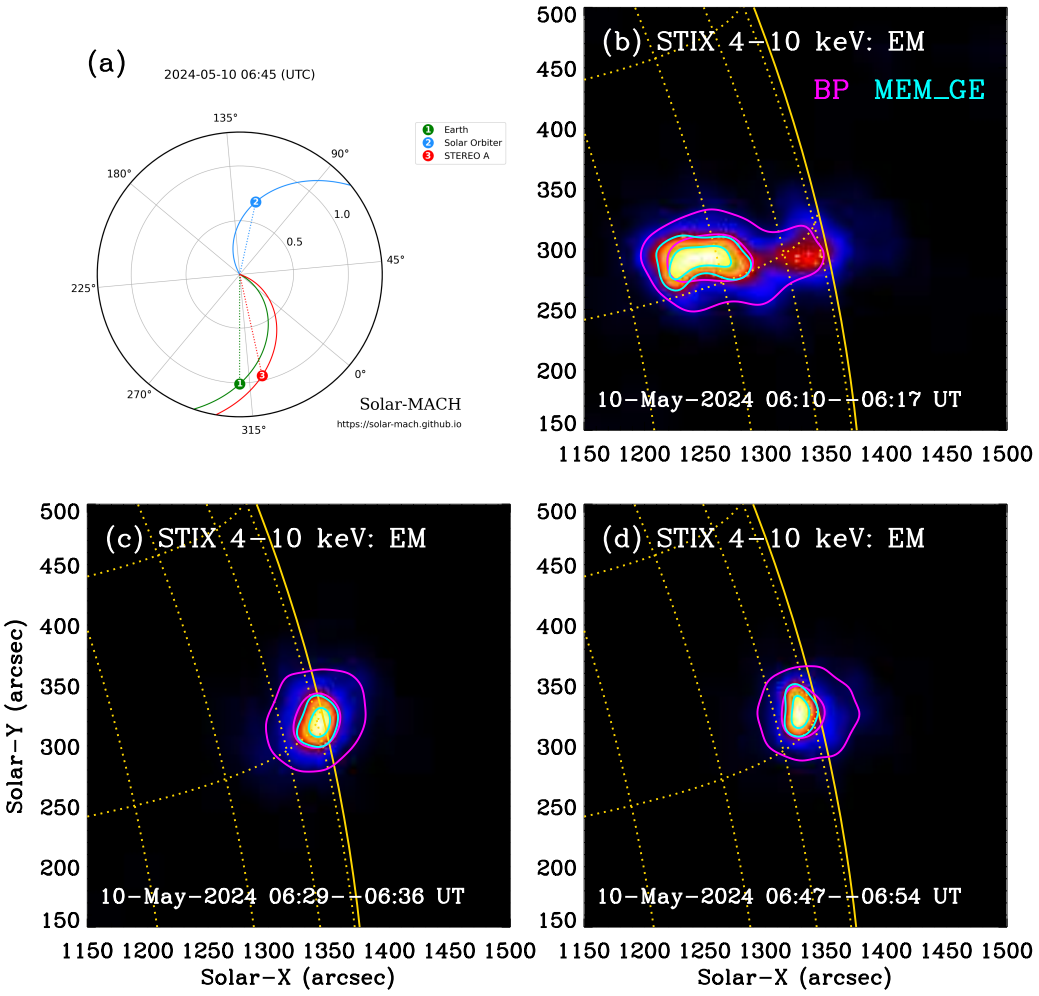

Figure 10. (a): Sketch plot of the spatial locations of Solar Orbiter and STEREO_A and their connections with the Sun and Earth. (b) Reconstructed STIX images at 4-10 keV using three algorithms (EM, BP, and MEM_GE). The contour levels are set at 50% and 80%. The dotted gold lines represent latitude-longitude grids, and the solid gold line marks the solar limb.

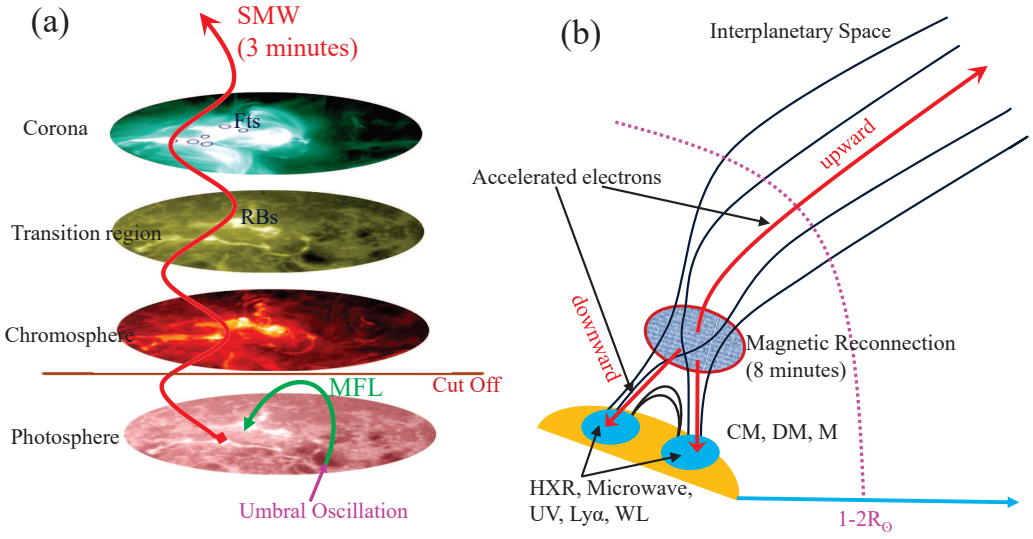

Figure 11. Cartoon images for illustrating the origin of flare QPPs. (a): The 3-min period is modulated by the slow magnetoacoustic wave (SMW), which is originating from the umbral oscillation in the sunspot. It propagates along the magnetic field line (MFL) to the flare area, i.e., two ribbons (RBs) or double footpoints (Fts). Here, the low-frequency cutoff prevents long-period wave propagating from the photosphere to the upper atmosphere. (b): The 8-min period is possibly triggered by the repeated magnetic reconnection, which may periodically accelerate non-thermal electrons. In this process, double footpoints are formed in the HXR/microwave channels, two ribbons or some kernels are generated in the UV, Lyα, and white-light (WL) emissions, and a group of radio bursts can be seen in various frequencies of centimeter (CM), decimeter (DM) and meter(M) regimes, or the low frequency in the interplanetary space.